CSIRO PUBLISHING

Invertebrate Systematics, 2019, **33**, 697–717
https://doi.org/10.1071/IS19002

The anatomy of an unstable node: a Levantine relict precipitates phylogenomic dissolution of higher-level relationships of the armoured harvestmen (Arachnida: Opiliones: Laniatores)

Shlomi Aharon[A], *Jesus A. Ballesteros*[B], *Audrey R. Crawford*[B], *Keyton Friske*[B], *Guilherme Gainett*[B], *Boaz Langford*[C], *Carlos E. Santibáñez-López*[B], *Shemesh Ya'aran*[C], *Efrat Gavish-Regev*[A,D] *and Prashant P. Sharma*[B,D]

[A]The Arachnid National Natural History Collection, The Hebrew University of Jerusalem, Edmond J. Safra Campus, Givat Ram, Jerusalem 9190401, Israel.
[B]Department of Integrative Biology, University of Madison-Wisconsin, 352 Birge Hall, 430 Lincoln Drive, Madison, WI 53706, USA.
[C]Israel Cave Research Center, Institute of Earth Sciences, The Hebrew University of Jerusalem, Edmond J. Safra Campus, Givat Ram, Jerusalem 9190401, Israel.
[D]Corresponding authors. Email: efrat.gavish-regev@mail.huji.ac.il; prashant.sharma@wisc.edu

Abstract. After tumultuous revisions to the family-level systematics of Laniatores (the armored harvestmen), the basally branching family Phalangodidae presently bears a disjunct and irregular distribution, attributed to the fragmentation of Pangea. One of the curious lineages assigned to Phalangodidae is the monotypic Israeli genus *Haasus*, the only Laniatores species that occurs in Israel, and whose presence in the Levant has been inferred to result from biogeographic connectivity with Eurasia. Recent surveys of Israeli caves have also yielded a new troglobitic morphospecies of *Haasus*. Here, we describe this new species as *Haasus naasane* sp. nov. So as to test the biogeographic affinity of *Haasus*, we sequenced DNA from both species and RNA from *Haasus naasane* sp. nov., to assess their phylogenetic placement. Our results showed that the new species is clearly closely related to *Haasus judaeus*, but *Haasus* itself is unambiguously nested within the largely Afrotropical family Pyramidopidae. In addition, the Japanese 'phalangodid' *Proscotolemon sauteri* was recovered as nested within the Southeast Asian family Petrobunidae. Phylogenomic placement of *Haasus naasane* sp. nov. in a 1550-locus matrix indicates that Pyramidopidae has an unstable position in the tree of Laniatores, with alternative partitioning of the matrix recovering high nodal support for mutually exclusive tree topologies. Exploration of phylogenetic signal showed the cause of this instability to be a considerable conflict between partitions, suggesting that the basal phylogeny of Laniatores may not yet be stable to addition of taxa. We transfer *Haasus* to Pyramidopidae (new familial assignment). Additionally, we transfer *Proscotolemon* to the family Petrobunidae (new familial assignment). Future studies on basal Laniatores phylogeny should emphasise the investigation of small-bodied and obscure groups that superficially resemble Phalangodidae.

Additional keywords: Assamioidea, Grassatores, *Haasus*, Petrobunidae, Phalangodidae, *Proscotolemon*, Pyramidopidae.

Received 10 January 2019, accepted 28 March 2019, published online 3 October 2019

Introduction

The era of phylogenomics proffers the tantalising promise of resolving the most challenging puzzles in the Tree of Life. The acquisition of large quantities of molecular sequence data is anticipated to increase the dispositive power of datasets, although controversies, both historical and new, abound as to how datasets should be assembled (Rokas 2005; Wiens 2006; Wiens and Tiu 2012; Roure *et al*. 2013; Salichos and Rokas 2013), as well as which analyses should be performed to account for an array of systematic errors (Dequeiroz and Gatesy 2007; Song *et al*. 2012; Gatesy and Springer 2014; Simmons and Gatesy 2015; Tonini *et al*. 2015; Kocot *et al*. 2016; Feuda *et al*. 2017; Shen *et al*. 2017). Numerous phylogenetic nodes have been resolved through the application of genome-scale

datasets to various taxonomic ranks, abetted by the development of scalable algorithmic and analytical approaches (Minh *et al*. 2013; Aberer *et al*. 2014; Kück and Struck 2014; Kozlov *et al*. 2015; Mirarab and Warnow 2015; Nguyen *et al*. 2015).

In spite of these advances, the meaning of 'phylogenomic resolution' merits some scrutiny. Myriad empirical works proclaim the achievement of phylogenomic resolution, which is typically assessed using some combination of high nodal support (e.g. bootstrap resampling frequency; posterior probability) and insensitivity to parameter variation (e.g. Sharma *et al*. 2015; Fernández *et al*. 2017; Schwentner *et al*. 2017). However, the criterion of support from resampling techniques has proven problematic in empirical datasets; given the scale of some phylogenomic datasets, alternative partitioning can yield maximal nodal support for mutually exclusive topologies because of the amplification of inherent biases, especially when short internodes are present deep in evolutionary time (Sharma *et al*. 2014; Kocot *et al*. 2016; Linkem *et al*. 2016). It has recently also shown that even a few anomalous partitions can skew analyses of supermatrices (Shen *et al*. 2017). As for sensitivity analyses, while it is generally agreed that exploration of datasets is a prerequisite for robust phylogenetic inference, there are few prescriptions as to which dimensions of phylogenetic data should be explored and to what degree. Phylogenomic datasets have historically focussed on taxon occupancy (the trade-off between dataset size and dataset density) as a primary axis for investigation, because of rightful concerns about the influence of missing data, but other variables such as evolutionary rate, completeness of sequences, compositional heterogeneity, heterotachy, and phylogenetic informativeness have all been shown to influence empirical datasets, resulting in a heavy inferential burden. Even with intensive investigation of parameter space, there exists no clear bright-line for 'phylogenomic resolution' in sensitivity analyses, when subsets of analyses disagree with the most commonly recovered hypothesis (Sharma *et al*. 2014; Schwentner *et al*. 2017).

We examined herein a test case of an arthropod group to which the attribute of clear phylogenomic resolution has been historically applied, namely, Opiliones (commonly known as 'daddy-long-legs' or 'harvestmen'), the third largest order of chelicerate arthropods. The characterisation of their resolution largely pertains to the relationships of their four constituent extant suborders (in an increasing order of diversity: Cyphophthalmi, Dyspnoi, Eupnoi, Laniatores), which were once contentious in analyses of 2–10 genes (Giribet *et al*. 1999, 2002, 2010; Shultz and Regier 2001) and, subsequently, resolved by a phylogenomic analysis of eight Opiliones taxa (Hedin *et al*. 2012). The first phylogenomic analysis that sampled multiple families within each suborder recovered stable subordinal relationships with high nodal support (Fernández *et al*. 2017). In spite of this, a handful of families were not sampled in the most recent analysis, including two families of Laniatores, namely, Tithaeidae (Sharma and Giribet 2011; Sharma *et al*. 2017; Schmidt *et al*. 2019) and Pyramidopidae (Sharma *et al*. 2011). These families are compelling for two reasons. First, their phylogenetic affinities are uncertain, as inferred from analyses of a 10-locus legacy Sanger dataset (Sharma *et al*. 2017); in the case of pyramidopids, even superfamilial assignment is questionable (Sharma and Giribet 2011; Cruz-López *et al*. 2016). Second, the region where these two families are anticipated to fall in the Laniatores tree of life is fraught with short internodes as previously noted by Sharma and Giribet (2011), a phenomenon that was not explored by Fernández *et al*. (2017). Concordantly, it was in this part of the Opiliones phylogeny of Fernández *et al*. (2017) where nodes were, in fact, demonstrably less stable than what would merit the affirmative title of phylogenomically 'resolved' or 'stable' (between 25% and 87.5% of analyses incongruent with, or failing to support, the preferred tree topology depicted; compare fig. 1 and fig. S2 of Fernández *et al*. 2017). As such, the claim of phylogenomic resolution of Opiliones belies marked uncertainty of such nodes as the monophyly of the Laniatores superfamily Epedanoidea, the paraphyly of Samooidea, and the identity of the sister group of the remaining Gonyleptoidea (in addition to the monophyly of the Cyphophthalmi family Sironidae).

Propitiously, in pursuit of neglected groups of small-bodied Laniatores previously assigned to the wastebasket family Phalangodidae, we discovered, in a cave in Israel (Frumkin *et al*. 2018), a new troglobitic morphospecies resembling the phalangodid genus *Haasus* Roewer, 1949, a monotypic lineage also endemic to Israel (Roewer 1949). On characterising the phylogenetic placement of both species, we quickly discovered that *Haasus* was, in fact, not a phalangodid, but was more closely allied to Pyramidopidae, a group previously also thought to be a lineage of phalangodids (Sharma *et al*. 2011). This parallels the recent discovery of the first Neotropical troglobitic pyramidopid in Belise, which was previously mistaken for a stygnommatid (Cruz-López *et al*. 2016). We, therefore, sequenced the transcriptome of this new species, anticipating improved resolution of the unstable nodes inherent in the analysis of Fernández *et al*. (2017).

Here, we describe the morphospecies in question, substantiate its identification as a pyramidopid, and demonstrate systemic conflict in its phylogenomic placement. Our results provide an interesting test case where increasing the taxon sampling, even by a single terminal, incurred a new short internode in the phylogeny and, thus, destabilised phylogenomic relationships.

Materials and methods

Taxonomy

Examined specimens have been deposited in the following institutions: HUJ (The Arachnid National Natural History Collection, The Hebrew University of Jerusalem, Jerusalem, Israel), UW (Museum of Zoology, University of Wisconsin-Madison, Madison, WI, USA), MCZ (Museum of Comparative Zoology, Harvard University, Cambridge, MA, USA), ZMUC (Zoological Museum, University of Copenhagen, Copenhagen, Denmark) and MHNG (Muséum d'Histoire Naturelle, Genève, Switzerland).

The holotype and a female paratype of the new species were photographed using a Canon MP-E65 X5 macro lens-equipped digital colour camera (Canon, Tokyo, Japan). Multiple specimens were examined with a Quanta FEI 200 scanning electron microscope (SEM) (Quanta, FEI, Hillsboro, OR, USA). The genitalia of male and female paratypes were also

examined by SEM. Specimens previously used for DNA extraction are indicated as such among the type material. Methods concerning molecular-sequence data obtained from these specimens are described below. All measurements are given in millimetres, unless otherwise indicated. Nomenclature on cuticular ornamentation follows (Murphree 1988).

The following type material was examined for comparison:

Haasus judaeus Roewer, 1949: ISRAEL: two ♂, three ♀, paratypes, northern Tel Aviv, xii.1937, unknown leg. (HUJ INVOP 501-505).

Molecular methods and dataset assembly

Methods for DNA extraction, amplification and Sanger sequencing follow our published procedures (Sharma and Giribet 2009, 2011). One specimen each of *Haasus judaeus* and *H. naasane* sp. nov., as well as several morphospecies of Gabonese Pyramidopidae, were extracted using Qiagen DNEasy Blood and Tissue Kit (Qiagen, Valencia, CA, USA). Locality and accession data are provided in Table 1. Molecular markers amplified and sequenced consisted of two nuclear ribosomal genes (18S rRNA and 28S rRNA), two nuclear protein-encoding genes (histone H3 and histone H4), and one mitochondrial ribosomal gene (16S rRNA). Primer sequences have been provided in Sharma and Giribet (2011) and GenBank/NCBI accession data in Table 2. Chromatograms were read and sequences assembled using the sequence-editing software Geneious R9. Sequence data were inspected for errors in Seaview v. 4.7 (Gouy *et al*. 2010) and added to the 10-locus dataset of Laniatores assembled by Sharma and Giribet (2011), with the modification that the more variable first fragment of 28S rRNA was not included (absent for newly sequenced terminals) and previously detected contaminations were excluded (as detailed by Cruz-López *et al*. 2016; Sharma *et al*. 2017). *De novo* sequence alignment was performed using MUSCLE v. 3.6 (Edgar 2004), with trimming of ambiguously aligned regions by using Gblocks v. 0.91b (Castresana 2000). The ensuing dataset is, henceforth, termed ‘Matrix 1’.

Additionally, two species were added to the dataset and analysed in a separate family of analyses, because of a significant unavailability of sequence data for both terminals. These were *Maiorerus randoi* (a pyramidopid from the Canary Islands, represented only by complete 18S rRNA (U37004) and a 352-bp fragment of 28S rRNA (GenBank U91505)) and *Proscotolemon sauteri* (a phalangodid from Japan, represented only by elongation factor 1α (EF-1α; GenBank AF240872), a 915-bp fragment of 28S rRNA from the variable first fragment (GenBank LC041003), and cytochrome *c* oxidase subunit I (COI; GenBank AB937961)). This dataset incorporated the variable first fragment of 28S rRNA that was excluded from Matrix 1, so as to inform the placement of *Proscotolemon sauteri*. The ensuing dataset is, henceforth, termed ‘Matrix 2’.

Total RNA was extracted from a single specimen of *Haasus naasane* sp. nov. by using a TRI Reagent (ThermoFisher). Messenger RNA purification, library preparation, and 2 × 100 sequencing on an Illumina HiSeq 2500 platform follow our previous procedures (Sharma *et al*. 2014). Transcriptome assembly was performed using Trinity v. 2.8 (Grabherr *et al*.

Table 1. Accession numbers and locality data for sequenced terminals

Species	Specimens	Voucher number	Locality	Coordinates	Date	Collector
Haasus						
Haasus naasane sp. nov.	1 juvenile		A’rak Na’asane Cave, Israel	31.994938°N, 35.407476°E	31.xii.2017	S. Aharon, A. Frumkin, B. Langford
Haasus naasane sp. nov.	1 male, 2 females		A’rak Na’asane Cave, Israel	31.994938°N, 35.407476°E	7.viii.2018	S. Aharon, G. Gainett, J. Ballesteros
Haasus judaeus	1 male		Nahal Oren, Israel	32.713°N, 34.975°E	10.vi.2017	P. Sharma, A. Chipman, Y. Lubin, E. Gavish-Regev
Sorensenius						
Sorensenius sp. As020	1 male	MCZ IZ 127913	Reserve du Plateau d’Ipassa, Makokou, Ogooué-Ivindo, Gabon	0.511766667°N, 12.8001°E	24.vi.2009	L. Benavides, G. Giribet, J. Mavoungou, J. Murienne
Sorensenius sp. As022	1 male	MCZ IZ 127912	Reserve du Plateau d’Ipassa, Makokou, Ogooué–Ivindo, Gabon	0.511766667°N, 12.8001°E	24.vi.2009	L. Benavides, G. Giribet, J. Mavoungou, J. Murienne
Sorensenius sp. As026	1 male	MCZ IZ 127912	Reserve du Plateau d’Ipassa, Makokou, Ogooué-vindo, Gabon	0.511766667°N, 12.8001°E	24.vi.2009	L. Benavides, G. Giribet, J. Mavoungou, J. Murienne
Sorensenius sp. As030	1 male	MCZ IZ 127912	Reserve du Plateau d’Ipassa, Makokou, Ogooué-Ivindo, Gabon	0.50745°N, 12.79673333°W	24.vi.2009	L. Benavides, G. Giribet, J. Mavoungou, J. Murienne
Sorensenius sp. As038	1 male	MCZ IZ 127932	Reserve du Plateau d’Ipassa, Makokou, Ogooué-Ivindo, Gabon	0.504483333°N, 12.79525°W	25.vi.2009	L. Benavides, G. Giribet, J. Mavoungou, J. Murienne
Sorensenius sp. As041	1 male	MCZ IZ 127931	Kéri, Moyen Ogooué, Gabon	0.751366667°S, 10.37756667°W	28.vi.2009	L. Benavides, G. Giribet, J. Murienne

Table 2. GenBank accession numbers for new sequence data of Pyramidopidae

Species	Accession #	18S rRNA	28S rRNA	16S rRNA	COI	H3	H4	SRA BioProject	SRA BioSample
Haasus									
Haasus naasane sp. nov.								PRJNA540868	SAMN11567271
Haasus naasane sp. nov.		MN169029	MN169037	MN169020		MN169050	MN169052		
Haasus judaeus		MN169030	MN169038	MN169019		MN169049	MN169051		
Sorensenius									
Sorensenius sp. As020	MCZ IZ 127913	MN169023	MN169031	MN169021	MN169039	MN169044			
Sorensenius sp. As022	MCZ IZ 127912	MN169024	MN169032		MN169040				
Sorensenius sp. As026	MCZ IZ 127912	MN169025	MN169033		MN169041	MN169045			
Sorensenius sp. As030	MCZ IZ 127912	MN169026	MN169034		MN169042	MN169046			
Sorensenius sp. As038	MCZ IZ 127932	MN169027	MN169035	MN169022		MN169047			
Sorensenius sp. As041	MCZ IZ 127931	MN169028	MN169036		MN169043	MN169048			

2011). To expedite phylogenomic inference, a set of 1550 orthologs previously established for inference of Opiliones relationships was selected for analysis (Fernández *et al*. 2017). The alignment was broken into individual partitions by using a series of custom Python scripts. Orthologs of *Haasus naasane* sp. nov. were identified with a tBLASTn search, followed by verification using the best reciprocal BLAST hit. These were added to their corresponding partition, with *de novo* sequence alignment using MUSCLE v. 3.6 (Edgar 2004) and trimming of overhanging sites by using Gblocks v. 0.91b (Castresana 2000), culminating in 'Matrix 3'.

To explore the relationship between data-matrix completeness and phylogenetic robustness, we constructed additional matrices by varying the threshold for gene occupancy. On doing so, we discovered discrepancies in the work of Fernández *et al*. (2017), pertaining to the design of phylogenomic matrices. The 1550-gene matrix was previously described as retaining >50% taxon occupancy per partition by Fernández *et al*. (2017); on reanalysing that dataset, we discovered that only 1414 orthologs bore >50% taxon occupancy (>33 of 67 taxa). The 304-locus matrix with >75% occupancy described by Fernández *et al*. (2017) was also erroneous; we found only 210 genes with >75% taxon occupancy (>60 of 67 taxa). Finally, the 78-gene matrix previously described as retaining >90% taxon occupancy was discovered to have much higher missing data than reported; we found that a paltry 14 genes in the matrix of Fernández *et al*. (2017) actually met the criterion of >90% gene occupancy (Fig. S1, available as Supplementary material to this paper).

We, therefore, redesigned additional matrices as follows, towards correcting the errors of Fernández *et al*. (2017), while also systematically dissecting the effects of missing data. As such, we created datasets of 1414 genes (>50% taxon occupancy (>33 taxa); henceforth, 'Matrix 4'), 304 genes (>70% taxon occupancy (>47 taxa); 'Matrix 5′), 210 genes (>75% taxon occupancy (>50 taxa); 'Matrix 6'), 101 genes (>80% taxon occupancy (>54 taxa); 'Matrix 7'), 78 genes (>55 taxa; 'Matrix 8'), and 14 genes (more than 90% gene occupancy (>60 taxa); 'Matrix 9'). Three additional matrices were separately analysed (>35 taxa, >40 taxa, >45 taxa), but were incorporated only in analyses of quartet mapping and comparison of constituent loci, so as to reduce redundancy (see below). The occupancy proportions were calculated before the addition of *Haasus naasane* sp. nov., to redress previous oversights (Fernández *et al*. 2017).

All 12 aligned datasets are provided as supplementary material. Numbers of genes per taxon in every matrix, as well as the proportion of missing data (as a proportion of sites) in each matrix's, are reported in Table S1 (available as Supplementary material to this paper).

Phylogenetic analyses

Maximum-likelihood (ML) analyses were conducted using RAxML v. 8.2 (Stamatakis 2014) for the 10-locus dataset. A unique GTR model of sequence evolution, with corrections for a discrete gamma distribution, was specified for each data partition and 500 independent searches were implemented. Nodal support was estimated via the rapid bootstrap algorithm, with 500 replicates (Stamatakis *et al*. 2008) for Datasets 1 and 2.

For the phylogenomic datasets (Datasets 3–9), ML analyses were performed in IQ-TREE v. 1.5.5 (Nguyen *et al*. 2015), by using inbuilt tools for model selection and implementing 1000 ultrafast bootstrap resampling replicates to assess nodal support (Nguyen *et al*. 2015; Kalyaanamoorthy *et al*. 2017; Hoang *et al*. 2018). A separate set of ML analyses was performed using ExaML v. 3 (Kozlov *et al*. 2015), to facilitate replicability of the main analyses of Fernández *et al*. (2017). Species tree estimation of the constituent orthogroups of the three matrices were generated using ML gene-tree topologies inferred using RAxML v. 8.2, with downstream analysis using ASTRAL-II (Mirarab and Warnow, 2015). Quartet mapping was performed using inbuilt tools in IQ-TREE v. 1.5.5. Dominant bipartitions among the ML gene-tree topologies were visualised by constructing super-networks using the SuperQ method (Grünewald *et al*. 2013), using all 1550 gene trees as inputs.

Bayesian inference (BI) analysis was conducted using MrBayes v. 3.2 (Ronquist *et al*. 2012) for Dataset 1, implementing a unique GTR model of sequence evolution, with corrections for a discrete gamma distribution and for invariant sites, following our previous model-fitting for this dataset (Sharma and Giribet 2011). Four runs, each with four chains and the default distribution of chain temperatures, were implemented for 2×10^7 generations. Assessment of chain mixing and convergence diagnostics were performed using Tracer v. 1.7 and inbuilt tools in MrBayes v. 3.2. As a

conservative measure, 4×10^6 generations (20%) were discarded from each chain as burn-in.

Molecular dating

Estimation of divergence times was conducted using BEAST v. 1.8 (Drummond *et al*. 2006; Drummond and Rambaut 2007); Matrix 2 was selected for analysis because of its richness of taxonomic sampling. We specified a unique GTR model of sequence evolution, with corrections for a discrete gamma distribution and a proportion of invariant sites (GTR + Γ + I) for each partition; protein-coding genes were further partitioned with two separate site models, for first and second positions versus the third codon position. Model selection followed the results of model testing as implemented in Sharma and Giribet (2011) and Giribet *et al*. (2012). Fossil taxa were used to calibrate divergence times, as in previous studies (Garwood *et al*. 2014; Sharma and Giribet 2014; Schmidt *et al*. 2019). We constrained the age of Eupnoi and Dyspnoi by using truncated normal-distribution priors with a mean of 360 million years and a standard deviation of 30 million years, with the truncation set to 305 million years. These priors reflect the ages of the oldest crown group Eupnoi (*Macrogyion cronus* Garwood *et al*. 2011) and Dyspnoi (*Ameticos scolos* Garwood *et al*. 2011); the use of the truncated normal prior reflects a compromise between ages obtained using node- versus tip-dating strategies (Sharma and Giribet 2014). The age of Opiliones was constrained on the basis of the recently re-interpreted placement of the Devonian harvestman, *Eophalangium sheari* Dunlop *et al*. 2003*b* (see Dunlop *et al*. 2003*a*, 2003*b*; Garwood *et al*. 2014). A truncated normal-distribution prior with a mean of 430 and a standard deviation of 10, with the truncation set to 410 million years, was used to calibrate this node.

An uncorrelated lognormal clock model was applied to each partition, and a birth–death speciation process with incomplete sampling was assumed for the tree prior. Two Markov chains were run for 200 million generations, sampling every 20 000 generations. Convergence diagnostics were assessed using Tracer v. 1.7 (Rambaut and Drummond 2009).

Taxonomy

Order **OPILIONES** Sundevall, 1833.

Suborder **LANIATORES** Thorell, 1876.

Family **PYRAMIDOPIDAE** Sharma, Prieto and Giribet, 2011.

Type genus: *Soerensenius* (Loman, 1902), by subsequent designation: Kury, 2017: 19, 20).

Type species: *Soerensenius pygmaea* (Loman, 1902), by monotypy.

Genus ***Haasus*** Roewer, 1949.

Haasus naasane, sp. nov.

(Figs 1–4, 5*A*, *C*, *D*, *G*, *J*, *K*, Table 3)

Material examined

Holotype.

♂ (HUJINVOP 506), Israel, A'rak Na'asane Cave, 134 m alt. (cave entrance: 31.994938°N, 35.407476°E), leg. S. Aharon, G. Gainett, J. Ballesteros, 7.viii.2018.

Paratypes.

One ♂ and two ♀ (HUJ INVOP 507-509), in ethanol, same collecting data as holotype.

Four ♂ (HUJ INVOP 510-513), in ethanol, same locality as holotype, leg. S. Aharon, S. Ya'aran, Y. Aviksis, 12.xi.2017.

One ♂ and two ♀ (UW), in ethanol, same collecting data as holotype.

One ♂ and two ♀ (MCZ 153035-153036), in ethanol, same collecting data as holotype.

Two ♂ and one ♀ (MCZ 153037-153039), on SEM stubs, same locality as holotype, leg. S. Aharon, A. Frumkin, B. Langford, 31.xii.2017.

One ♂ and two ♀ (MHNG), in ethanol, same collecting data as holotype.

One ♂ and two ♀ (ZMUC NHMD188529), in ethanol, same collecting data as holotype.

Additional material studied

One juvenile extracted for DNA, same locality as holotype, leg. S. Aharon, A. Frumkin, B. Langford, 31.xii.2017.

One male, two females extracted for RNA from RNA*later*, same locality as holotype, leg. S. Aharon, S. Ya'aran, Y. Aviksis, 12.xi.2017.

Etymology

The specific epithet, a noun in apposition, is taken from the name of the cave that constitutes the type locality of this species. The locality name '*na*'*asane*', in turn, is the Arabic for 'sleepy' or 'sluggish', and pertains to the slow movement and appearance of this animal in comparison to its more active congener.

Diagnosis

Distinguished from *Haasus judaeus* Roewer, 1949 by (1) its greater body length, (2) paler color, (3) shorter and less protruding ocularium with eyes absent, (4) longer and more gracile palps, (5) pedipalpal claw shorter than pedipalpal tarsus, and (6) longer and more gracile walking legs.

Description

Total length of male holotype (female paratype in parentheses) 1.81 mm (1.72 mm), greatest width of prosoma 1.03 mm (0.95 mm), greatest width of opisthosoma 1.06 mm (1.17 mm); length-to-width ratio 1.75 (1.81). Body either trapezoidal (holotype) or campaniform (female) in shape, pale yellow in colour (in alcohol, depending on incidence of light), almost entirely with a dense microgranulate surface microstructure. Reduced eyes barely visible on well developed, triangular ocularium. Ocularium 0.54 mm (0.49 mm) long, 0.42 mm (0.4 mm) wide, with distal edge abutting anterior margin of carapace. Anterior margin of carapace without ornamentation. Scutal grooves of mesotergum indistinct. Free tergites granulated, unarmed.

Ventral prosomal complex (Fig. 3) of male and female, with coxae II and III meeting in midline, coxae I and IV not so. Anterior and posterior margins of coxae III without tubercular bridges to adjacent coxae. Genital operculum subtriangular, significantly larger in female than in male. Spiracles concealed in the male by posterior projecting pegs on coxa IV; barely visible in female. Opisthosomal sternites each with a regular belt of setose tubercles. Anal plate granulated, without tubercles.

Chelicerae (Fig. 4*A*) sexually monomorphic, with prominent bulla on proximal article. Proximal article with denticulate granulation basally and ventrally. Second article not

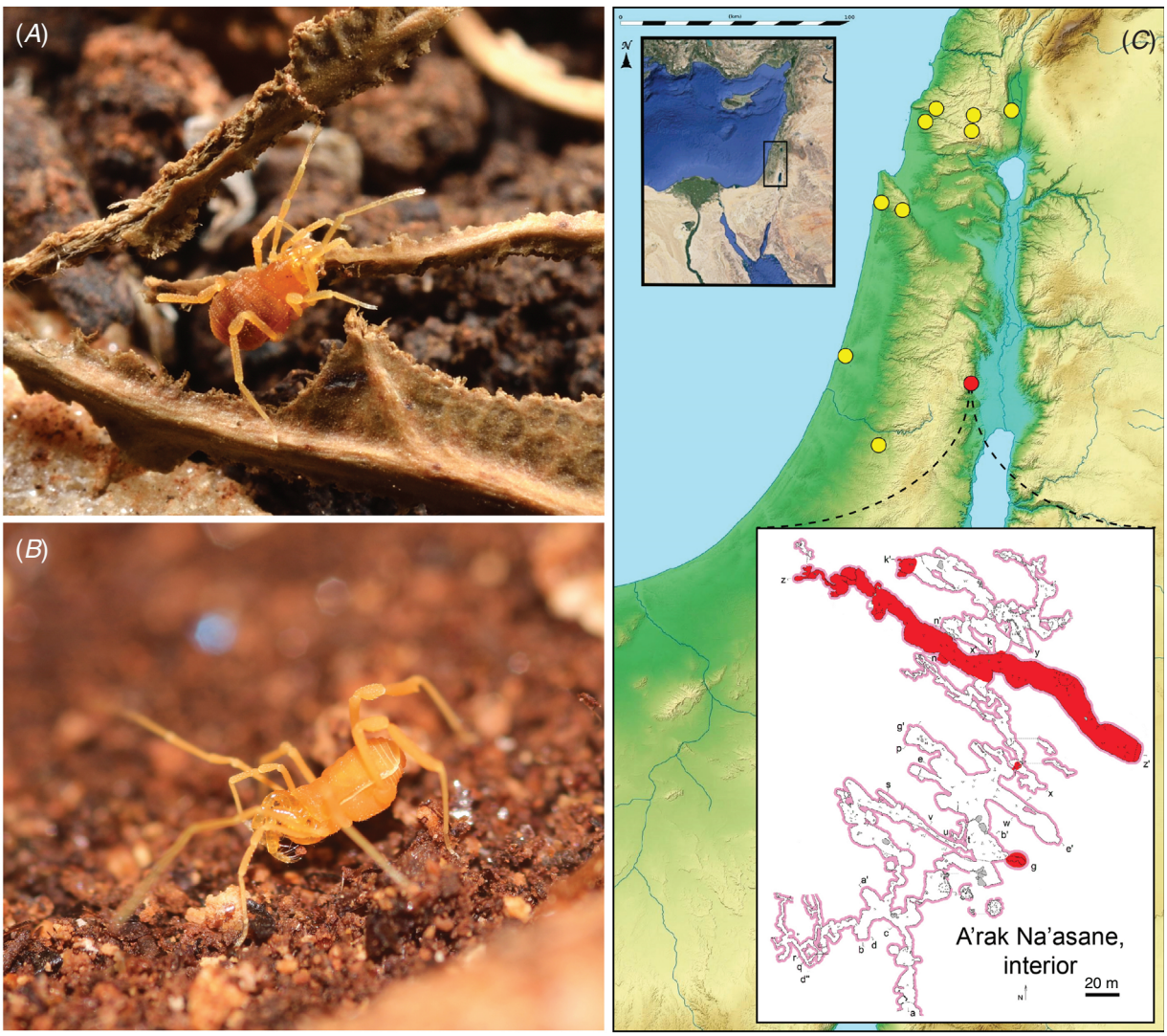

Fig. 1. Live habitus and distribution of *Haasus*. (*A*) Adult male of *Haasus judaeus* from exterior of Manot cave, Israel, photographed 18 July 2018 by J. Ballesteros. (*B*) Adult male of *Haasus naasane* sp. nov. from A'rak Na'asane cave, Israel, photographed 31 December 2017 by S. Aharon. (*C*) Map of the Levant, showing known localities of *Haasus judaeus* (yellow) and *Haasus naasane* sp. nov (red). Inset: interior map of A'rak Na'asane cav,e with detail of chambers found to contain *H. naasane* sp. nov. (red shading).

incrassate, free of ornamentation, with dorsal and latero-distal margin bearing several setae. Distal article with delicate dentition, free of ornamentation.

Palpi (Fig. 4*B*) robust and armed with large setose tubercles ventrally or ventrolaterally. Palpal trochanter with three setose tubercles, one larger than others. Palpal femur ventrally with two large proximal setose tubercles in a row, and three distal smaller setose tubercles; dorsally, with four setose tubercles of similar size, and one small distal setose tubercle; and with one large setose tubercle projecting mesally. Palpal patella with one large setose tubercle projecting mesally. Palpal tibia with two large setose tubercles projecting ectally, three large setose tubercles projecting mesally, two small setose tubercles on ectal surface and several setae. Palpal tarsus with two pairs of megaspines, several setae. Palpal claw nearly as long as palpal tarsus.

Legs I–IV (Fig. 4*C–G*) slender, elongate, finely granulated, with small and irregularly distributed setiferous tubercles on femora and tibiae. Sexually dimorphic row of large tubercles on the ventro-lateral margin of the patella and tibia of male leg IV (absence in the female), as well as more prominent setose tubercles on ventral margin of trochanter of male leg IV (reduced in the female). Tarsal claws I–IV smooth, unmodified, double claws on legs III and IV (typical of Grassatores). Tarsal formula 3 : 5 : 4 : 5.

Penis (Fig. 5*J*, *K*) elongate, narrow and slender, in the shape of a club. Ventral plate undivided, distally with two pairs of lateral setae and one pair of ventro-lateral setae. Proximally, at the widest portion, with four pairs of smaller lateral setae in a row. Basal sac extensible.

Sexual dimorphism

Female with comparatively smaller coxae of leg IV (Figs 1, 3*B*), significantly larger genital operculum (Fig. 3*D*), somewhat

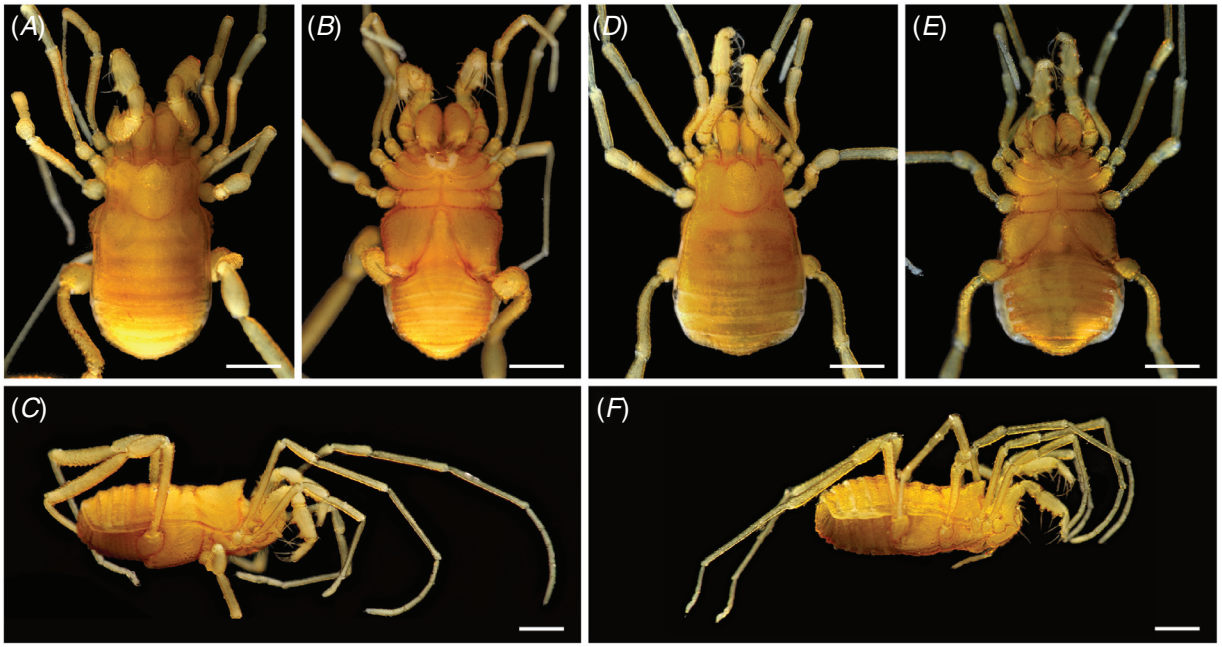

Fig. 2. *Haasus naasane* sp. nov. (*A*) Holotype, dorsal view. (*B*) Holotype, ventral view. (*C*) Holotype, lateral view. (*D*) Female paratype, dorsal view. (*E*) Female paratype, ventral view. (*F*) Female paratype, lateral view. Scale bar: 500 μm.

Fig. 3. *Haasus naasane* sp. nov. (*A*) Male paratype, ventral view. (*B*) Female paratype, ventral view. (*C*) Male paratype, prosomal complex. (*D*) Female paratype, prosomal complex. Scale bar: 500 μm.

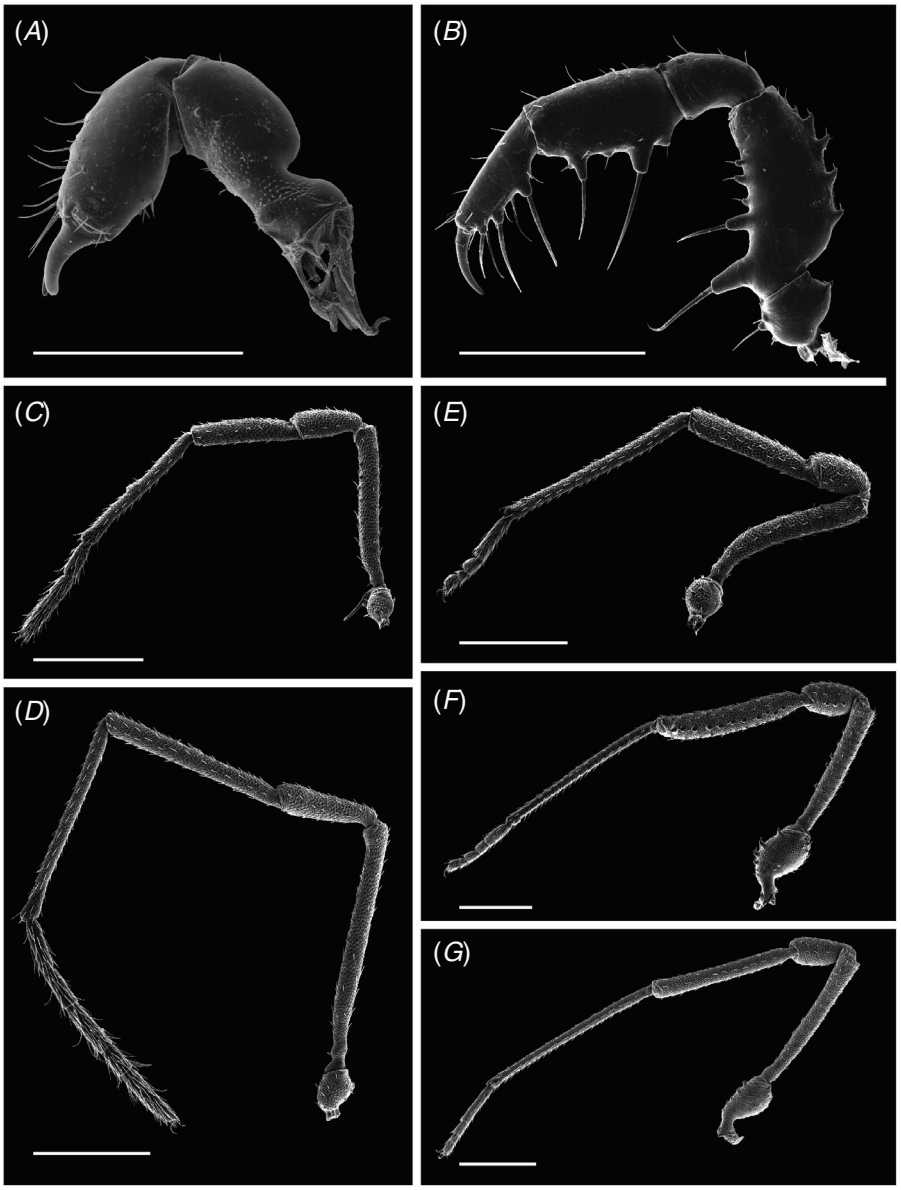

Fig. 4. *Haasus naasane* sp. nov. (*A*) Left chelicera of male paratype. (*B*) Left palp of male paratype. (*C*) Left leg I of male paratype. (*D*) Left leg II of male paratype. (*E*) Left leg III of male paratype. (*F*) Left leg IV of male paratype. (*G*) Left leg IV of female paratype. Scale bar: 500 µm.

Table 3. Appendage measurements of male paratype (MCZ 15037)
All measurements in mm

	Tr	Fe	Pa	Ti	Me	Ta	Total
Leg I	0.18	0.74	0.32	0.45	0.70	0.48	2.87
Leg II	0.19	1.08	0.44	0.80	0.91	1.08	4.50
Leg III	0.20	0.79	0.32	0.61	0.96	0.44	3.31
Leg IV	0.58	0.98	0.48	1.02	1.45	0.51	5.02
Palp	0.17	0.50	0.28	0.40		0.35	1.70
	Proximal	Second	Distal				
Chelicera	0.51	0.65	0.17				

smaller trochanter of leg IV, lacking bulbous tubercular rows on patella and tibia of leg IV, and four tarsomeres on leg IV (Fig. 4*G*).

Distribution and biogeography

Known only from type locality. *Haasus naasane* sp. nov. is a troglomorphic species, found in a single hypogene cave, A'rak Na'asane, which is located at the border between the semiarid eastern Samaria region and arid northern Judean desert (Frumkin *et al*. 2018). This hypogene cave was developed in Turonian limestone under a confined watertable condition during the Oligocene to Early Miocene. During the Late Eocene and Oligocene, regional upwarping brought about the uplift of southern and central Israel (Segev *et al*. 2011; Avni *et al*. 2012). Tectonic activity formed the Dead Sea Transform, which, together with the elevation of the Judean Mountains, caused the lowering of the watertable and drainage of the cave (Frumkin *et al*. 2017). Fluvial erosion formed deep canyons

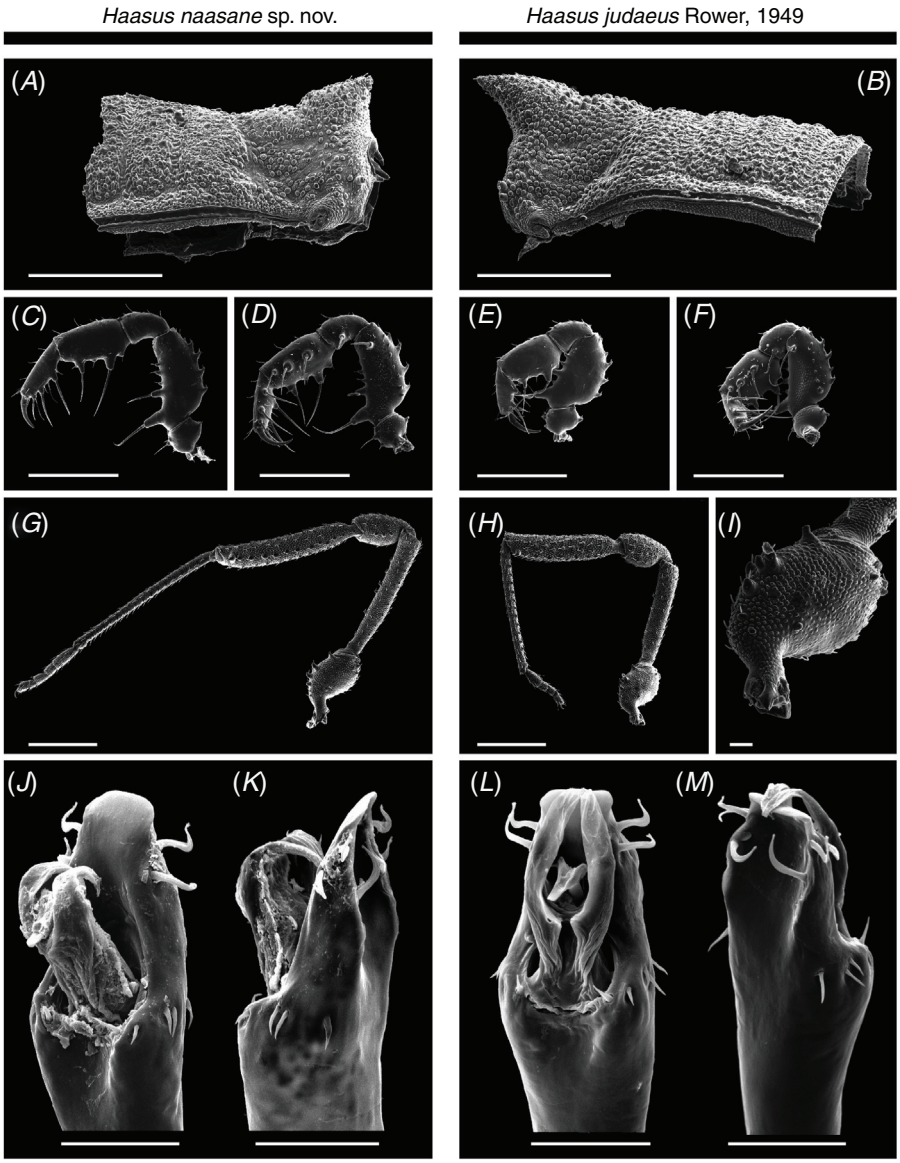

Fig. 5. Comparison of diagnostic characters in *Haasus judaeus* Roewer, 1949 (male) and *Haasus naasane* sp. nov. (male paratype). (*A*) Scutum of *H. naasane* sp. nov.; anterior is to the right. (*B*) Scutum of *H. judaeus*; anterior is to the left. (*C*) Left palp of *H. naasane* sp. nov. in ectal view. (*D*) Right palp of *H. naasane* sp. nov. in mesal view. (*E*) Left palp of *H. judaeus* in ectal view. (*F*) Right palp of *H. judaeus* in mesal view. (*G*) Left leg IV of *H. naasane* sp. nov. (*H*) Left leg IV of *H. judaeus*. (*I*) Detail of trochanter IV of *H. judaeus*. (*J*) Genitalia of *H. naasane* sp. nov. in dorsal view. (*K*) Genitalia of *H. naasane* sp. nov. in ventrolateral view. (*L*) Genitalia of *H. judaeus* in dorsal view. (*M*) Genitalia of *H. judaeus* in ventrolateral view. Scale bars: 500 µm (*A–H*), 40 µm (*I–M*).

running to the Dead Sea Rift Valley (DSRV), which exposed the cave entrance. The erosion rate of canyons at the DSRV has been extrapolated from canyons to the north and south to the cave area (Steinitz and Bartov 1992; Mor 1993); this mean rate is ~0.2 mm year^{-1}, where the entrance ceiling is ~10 m above the nearby wadi (river bed). It is, therefore, inferred that the cave entrance was formed ~50 000 years ago. It can be reasonably assumed that the connection between the cave and the surface was earlier than the age of the entrance; cracks and apertures can be used by arthropods to reach the underground before entrance creation.

This large cave (area: 8331 m^2) includes different microhabitats with a variety of humidity and temperature conditions. The temperature range is between 24°C and 26°C and the relative humidity range between 71.5% and 99.5% from the entrance to the deepest sections respectively (Frumkin *et al*. 2018). The sections of the cave where *H. naasane* was found are warm and humid inner chambers with a steady temperature of 25.7–26.1°C and a high relative humidity of 95.8–96.6% (Frumkin *et al*. 2018). In addition, these chambers are rich in organic matter and troglobitic arthropod fauna (with many undescribed morphospecies), as a result of the thick layer of

guano covering the cave floor, deposited by a colony of hundreds of *Asellia tridens* Geoffroy, 1813 (trident leaf-nosed bats). Adult and juvenile individuals of *Haasus naasane* sp. nov. were observed in all visits to the cave (March–November). Most of the individuals were found active on the guano, whereas a few were found active on the muddy ground, but never in the drier sections of the cave.

Results

Phylogenetic analysis of 10-locus nucleotide-sequence datasets

Both ML and BI analyses of Matrix 1 recovered the same relationships of Laniatores as previously obtained by Sharma and Giribet (2011), with maximal nodal support for the genus *Haasus* (Fig. 6*A*). Both *Haasus* terminals were recovered as nested within Pyramidopidae with support (bootstrap (BS) resampling frequency = 97%; posterior probability (PP) = 1.00). Internal relationships within Pyramidopidae were modestly supported, recovering a derived clade of afrotropical pyramidopids (BS = 82%; PP = 0.98), and *Jarmilana* and *Haasus* forming a grade with respect to the clade *Soerensenius* + *Conomma* (BS = 72%; PP = 95%). As in previous analyses (Sharma and Giribet 2011), Pyramidopidae was recovered as the sister group of Assamiidae in both ML and BI analyses, but with support only in BI analysis (PP = 1.00).

Two additional terminals represented by a paucity of sequence data were analysed in a separate dataset (Matrix 2) that spanned a larger fragment of 28S rRNA (the fastest-evolving partition of this locus, which also bore the most missing data). Maximum-likelihood analysis of Matrix 2 recovered the Canary Island pyramidopid *Maiorerus randoi* in a clade with the Neotropical troglobitic relict *Jarmilana pecki* (BS = 95%; Fig. 6*B*). In this tree topology, *Haasus* was recovered as the sister group of the clade *Jarmilana* + *Maiorerus*, with low support (63%). Separately, the same analysis recovered *Proscotolemon sauteri* as the sister group to two unidentified Petrobunidae from Taiwan (previously treated as two conspecific terminals of a Taiwanese morphospecies of *Petrobunus* by Sharma and Giribet (2011) and Zhang *et al*. (2018), with strong nodal support (BS = 100%; Fig. 6*C*). Despite the few sequence data available for *Proscotolemon* (314 bp, subsequent to alignment and trimming), the 28S rRNA of *Proscotolemon* is most similar to, yet distinct from, that of the Taiwanese petrobunids, differing at only 25 sites across this region. As a comparison, the same 314-bp region of 28S differed by 16 sites between *Petrobunus schwendingeri* and the Taiwanese petrobunids.

Both Matrices 1 and 2 were congruent with respect to other nodes in the Laniatores phylogeny.

Estimation of divergence times

Runs of BEAST reached stationarity after 27 million generations; 50 million generations (25%) were discarded as burn-in (Fig. 7). Inferred ages of diversification of key Laniatores lineages were consistent with our previous results (Sharma and Giribet 2011; Schmidt *et al*. 2019) and are not repeated here. The tree topology recovered by BEAST obtained the same relationships as obtained above, with a monophyletic *Haasus* being nested within Pyramidopidae, with maximal nodal support (Fig. 7), and *Proscotolemon* being nested within Petrobunidae, with maximal nodal support (not shown). Additionally, Assamiidae was recovered as the sister group of Pyramidopidae, with support.

The divergence of *Haasus* from the Atlantic group of pyramidopids (*Maiorerus* + *Jarmilana*) was estimated as 128.4 million years ago (95% highest posterior density (HPD) interval: 72.1–187.6 million years ago). The divergence of the two *Haasus* species was inferred to be 14.0 million years ago (95% HPD: 6.2–23.4 million years ago).

Phylogenomic analysis of peptide-sequence datasets

Maximum-likelihood analysis of Matrix 3 (1550 loci) yielded a tree topology with *Haasus naasane* sp. nov. as sister group to Gonyleptoidea, with maximal nodal support under either IQ-TREE v. 1.5.5 or ExaML v. 3 (Fig. 8). By contrast, a gene-tree reconciliation using ASTRAL-II recovered a different placement for *H. naasane* sp. nov., with this terminal forming a grade with the assamiid *Dampetrus* sp. with respect to Zalmoxoidea + Samooidea. Towards characterising the stability of *H. naasane* sp. nov. in the phylogenomic matrix, its placement was inferred across Matrices 3–9, using identical heuristic approaches for each dataset. Intriguingly, the clade Pyramidopidae + Gonyleptoidea was recovered only by the two largest matrices (Matrices 3 and 4) by using IQ-TREE v. 1.5.5, whereas ExaML v. 3 recovered this relationship for five of seven matrices (Matrices 3–6, 8) with varying levels of nodal support; ASTRAL-II recovered the clade Pyramidopidae + Gonyleptoidea only for Matrix 7. The two alternative placements for *H. naasane* sp. nov. most frequently recovered across the remaining analyses were as the sister group of *Dampetrus* sp. (the traditionally defined Assamioidea) and part of a grade with this assamiid species at the base of Zalmoxoidea + Samooidea (Fig. 8, inset). Recovery of Assamioidea (*H. naasane* sp. nov. + *Dampetrus* sp.) was variably supported by IQ-TREE v. 1.5.5 analysis in the four densest datasets (Matrices 6–9), but only in two matrices analysed using ExaML v. 3.

Quartet analysis and characterisation of the conflicting signal

To assess the discordance between the results of ASTRAL-II and concatenation methods in a way that obviated the confounding factor of missing data, quartet mapping was performed for two nodes in the tree. The first quartet comprised *H. naasane* sp. nov., *Dampetrus* sp. and one exemplar of each of Gonyleptoidea and Epedanoidea. This configuration was selected to span the alternative placements recovered for *H. naasane* sp. nov. in supermatrix and ASTRAL-II analyses. The second quartet consisted of a non-controversial node (the base of Grassatores), comprising the sandokanid *Gnomulus* sp., the phalangodid *Sitalcina lobata* and one exemplar of each of Gonyleptoidea and the clade Zalmoxoidea + Samooidea. This configuration was chosen for its parallels to the first quartet with respect to taxonomic sampling and data availability (one exemplar each of Sandokanidae, Phalangodidae, Assamiidae and Pyramidopidae).

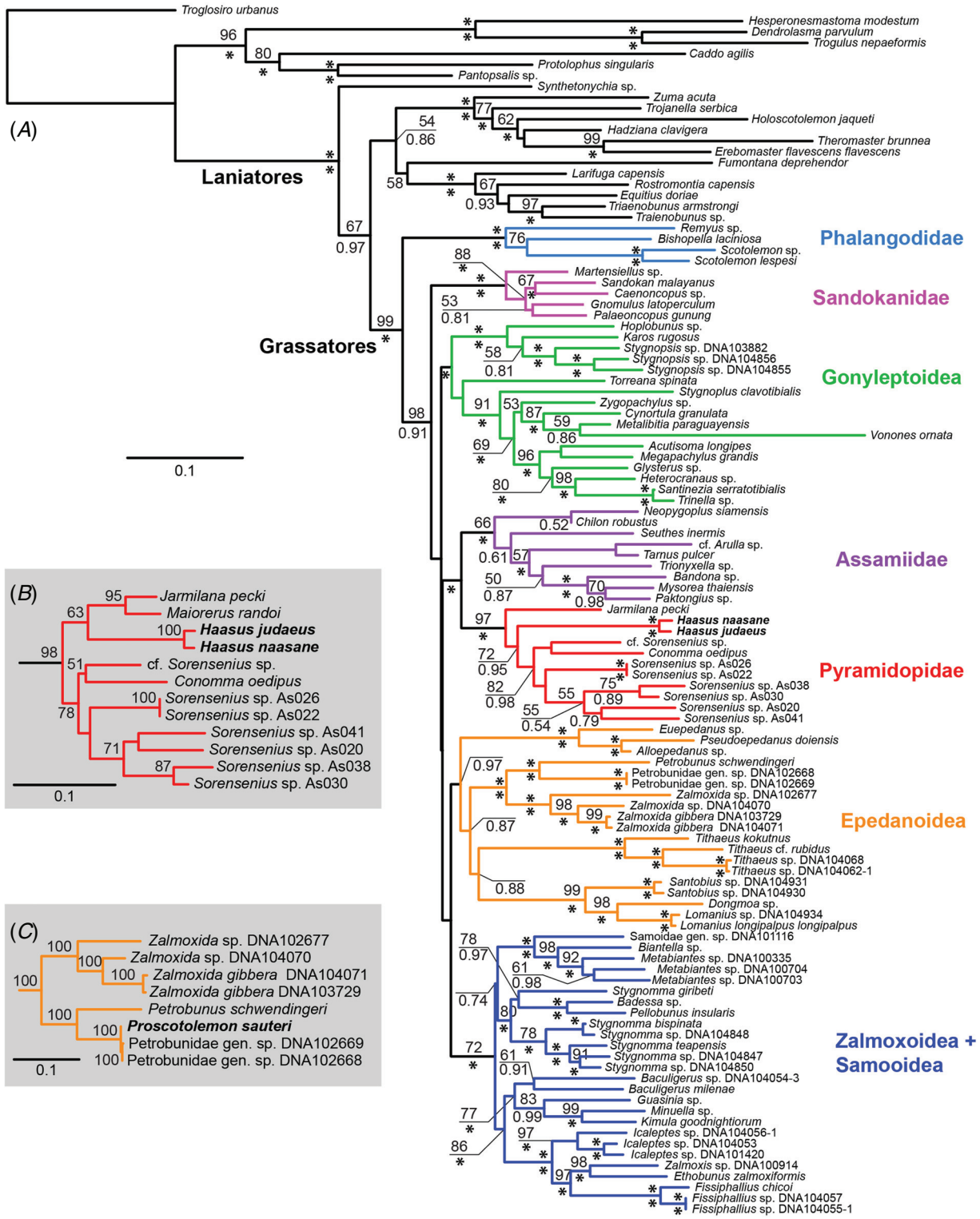

Fig. 6. Phylogenetic analyses of a 10-locus Sanger dataset. (*A*) Relationships of Laniatores inferred from maximum-likelihood analysis of Matrix 1 (lnL = –86 570.06). Numbers above nodes indicate bootstrap resampling frequencies. Numbers below nodes indicate posterior probabilities inferred from Bayesian inference analysis of all molecular data. (*B*) Relationships within Pyramidopidae inferred from maximum-likelihood analysis of Matrix 2 (lnL = –87 176.01), showing the placement of *Haasus* on inclusion of the data-poor terminal *Maiorerus randoi* (two loci). Numbers on nodes indicate bootstrap resampling frequencies. (*C*) Relationships within Petrobunidae from same analysis as in *B*, showing placement of the data-poor terminal *Proscotolemon sauteri* (one locus).

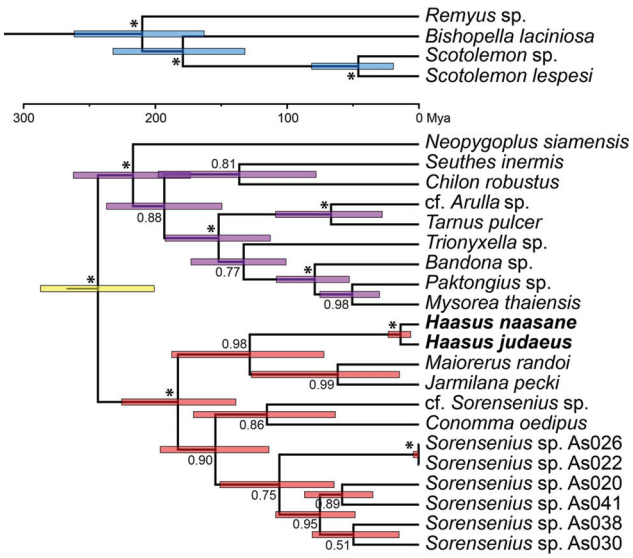

Fig. 7. Dated molecular phylogeny of Laniatores, showing lineages of interest (Phalangodidae (above); Assamioidea (below)). Bars on nodes indicate 95% highest posterior-density intervals. Numbers on nodes indicate posterior probability.

For the second, highly stable node (the base of Grassatores), quartet mapping using the entire 1550-locus supermatrix recovered the expected quartet (Gonyleptoidea and the clade Zalmoxoidea + Samooidea more closely related) for 100% of all possible quartets, with unambiguous support for the preferred topology (Fig. 9*A*). Sampling of quartets across individual loci in the matrix recovered a concordant result, with the majority of partitions proving to be uninformative (30.2%), and more than twice as many partitions supporting the expected topology as either alternative (26.8%).

By contrast, support for the quartets assessing the placement of *H. naasane* sp. nov. was similar for each of the three topologies (27.7–42.3%), on the basis of the complete 1550-gene supermatrix (Fig. 9*B*). Intriguingly, the quartet consistent with the clade Pyramidopidae + Gonyleptoidea received the least support. Sampling of quartets across all individual loci showed approximately equal support for each alternative topology (17.5–18.6%).

This family of analyses was conducted for all phylogenomic matrices (Matrices 3–9). The amount of support for each quartet as a function of supermatrix size was compared between the two nodes discussed above. The non-controversial node at the base of Grassatores showed the expected monotonic increase in the likelihood for the expected topology with an increasing number of genes (Fig. 9*C*). Even for the smallest matrix, support for the bipartition '*Sitalcina–Gnomulus*'–'Gonyleptoidea–Zalmoxoidea/Samooidea' was much higher than for the competing topologies. By contrast, the bipartition '*Haasus–Dampetrus*'–'Epedanoidea–Gonyleptoidea' was only modestly supported in smaller and denser matrices, with a loss of dispositive power of the supermatrix on the addition of genes (Fig. 9*D*). Similarly, the supernetwork of the partitions from Matrix 3 consisted of numerous reticulations and a star topology at the base of Grassatores (Fig. 10).

Discussion

The anatomy of a relict

The predilection for ascribing historical biogeographic modalities to various groups of Opiliones stems from a series of investigations into the evolutionary history of the suborder Cyphophthalmi (mite harvestmen). The phylogeny and temporal sequence of diversification of this taxon were shown to exhibit an unprecedented degree of fidelity to the geological history of the terranes it inhabits (Giribet and Boyer 2002; Boyer *et al*. 2007; Giribet *et al*. 2012; Sharma and Giribet 2014; Oberski *et al*. 2018). The textbook elegance and simplicity of vicariance as an explanatory vehicle for the distribution of one suborder invited its application to others, as molecular phylogenies became more available for various harvestmen lineages, particularly Laniatores (Giribet and Kury 2007; Giribet *et al*. 2010).

Phalangodidae was, thus, once considered to represent a Holarctic group (Giribet and Kury 2007; Giribet *et al*. 2010). Indeed, the distribution of Phalangodidae was explicitly attributed to Laurasian vicariance, because of the compelling inclusion of Nearctic and Eurasian endemics, as well as a single Japan species (*Proscotolemon*), a distribution paralleling that of the mite harvestman family Sironidae (Giribet and Kury 2007). Under this scenario, the presence of Holarctic opiliofauna in the Levant could have been attributed to a historically broadly distributed Palearctic lineage, whose range became fragmented with aridification of this region. This hypothesis is certainly consistent with the distribution of such Levantine harvestman endemics as *Dicranolasma hoberlandti* Silhavý, 1956, *Trogulus gypseus* Simon, 1879, *Nemastoma haasi* (Roewer, 1953), and various Holarctic genera within Eupnoi (Starega 1973), and would certainly have been consistent with the identity of *Haasus* as a Holarctic relict genus of Phalangodidae in Israel.

The Laurasian origin hypothesis was later emended on the discovery that the Malagasy genus *Remyus* (previously assigned to Zalmoxidae) was, in fact, a member of Phalangodidae, as inferred from a 10-locus phylogeny, wherein Phalangodidae was represented by just four terminals (Sharma and Giribet 2011). Because of the lack of a comprehensive internal phylogeny of Phalangodidae (i.e. sampling Holarctic taxa as well as *Remyus*, *Haasus* and *Proscotolemon*), we re-assembled here part of the two-gene (COI and 28S rRNA) dataset of Hedin and Thomas (2010) and included therein sequence data for *Haasus naasane* sp. nov., *Proscotolemon sauteri* and *Remyus* sp. The tree topology recovered retains *Remyus* sp. as the sister group of the remaining Phalangodidae, and shows that *Haasus* and *Proscotolemon* are not part of this clade (Fig. S2, available as Supplementary material to this paper).

On re-examining the morphology of *Haasus judaeus* and placing both *Haasus* terminals in a well sampled phylogenetic tree, we discovered that this genus is clearly a member of Pyramidopidae with unambiguous support (Figs 6, 7). This result is consistent with the external morphology of *Haasus* males (e.g. incrassate male coxa IV), previously noted as atypical for Phalangodidae (Ubick 2007), as well as the pars distalis of both *Haasus* species, which bear paired macrosetae typical of Pyramidopidae. The two species are demonstrably distinct, with *Haasus naasane*

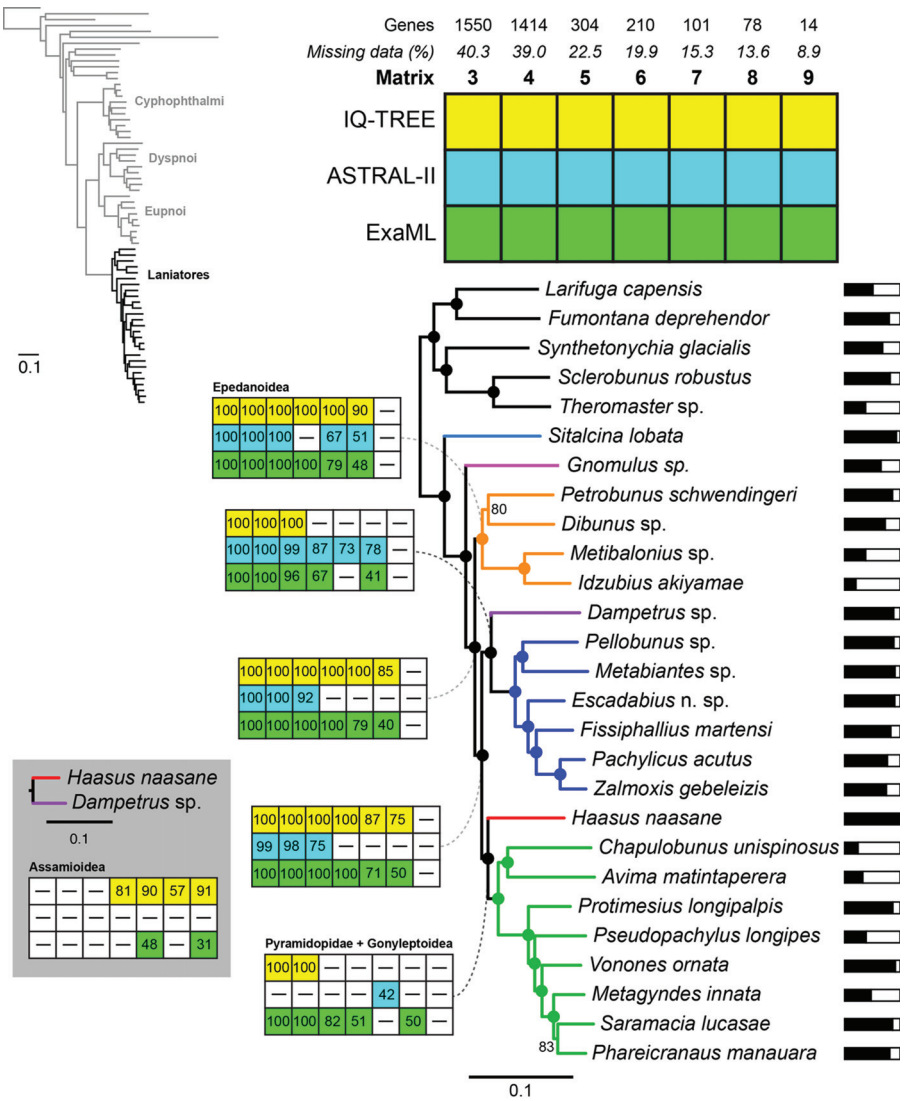

Fig. 8. Phylogenomic analyses of Opiliones. Supermatrix composition with numbers of genes and missing data, and accompanying methods (above). Relationships within Laniatores on the basis of maximum-likelihood analysis of 1550 loci (phylogeny of other suborders omitted for clarity; below, top left). Circles on nodes indicate maximal nodal support. Bars to the right of each terminal depict representation in data matrix (number of genes). Colours in branches correspond to Fig. 6. Coloured squares in sensitivity plots indicate recovery of a given node in the corresponding analysis, with nodal-support value indicated. Inset: Alternative topology, showing monophyly of Assamioidea.

sp. nov. exhibiting such characteristics of troglobitism as reduced eyes, longer palps and longer appendages (Fig. 5).

The recent split between the two *Haasus* species (estimated to have occurred between 6.2 and 23.4 million years ago), together with the prolonged gap between the origin and diversification of the genus (~115 million years), is consistent with the designation of this genus as a relict (Fig. 7). The type locality of *H. naasane* sp. nov. is a cave surrounded by deserts, with no contiguous habitats supporting humidity-dependent species such as *H. judaeus* (Fig. 1). We, therefore, infer that the two species have been geographically isolated at least since the aridification of this terrane. Biogeographically, the position of *Haasus* within Pyramidopidae, thus, suggests a novel historical scenario, with *Haasus* representing a relictual remnant of a largely afrotropical radiation, most of whose diversity is now restricted to Sub-Saharan Africa.

We, consequently, transfer *Haasus* to Pyramidopidae (*new familial assignment*). Paralleling this phylogenetic outcome, the few data available for *Proscotolemon sauteri* unambiguously place it within Petrobunidae, a family known from the Philippines, Sumatra, the Thai–Malay Peninsula, and mainland China (Sharma and Giribet 2011; Zhang *et al.* 2018). Specifically, *P. sauteri* was recovered as the sister group of an undescribed morphospecies of Petrobunidae,

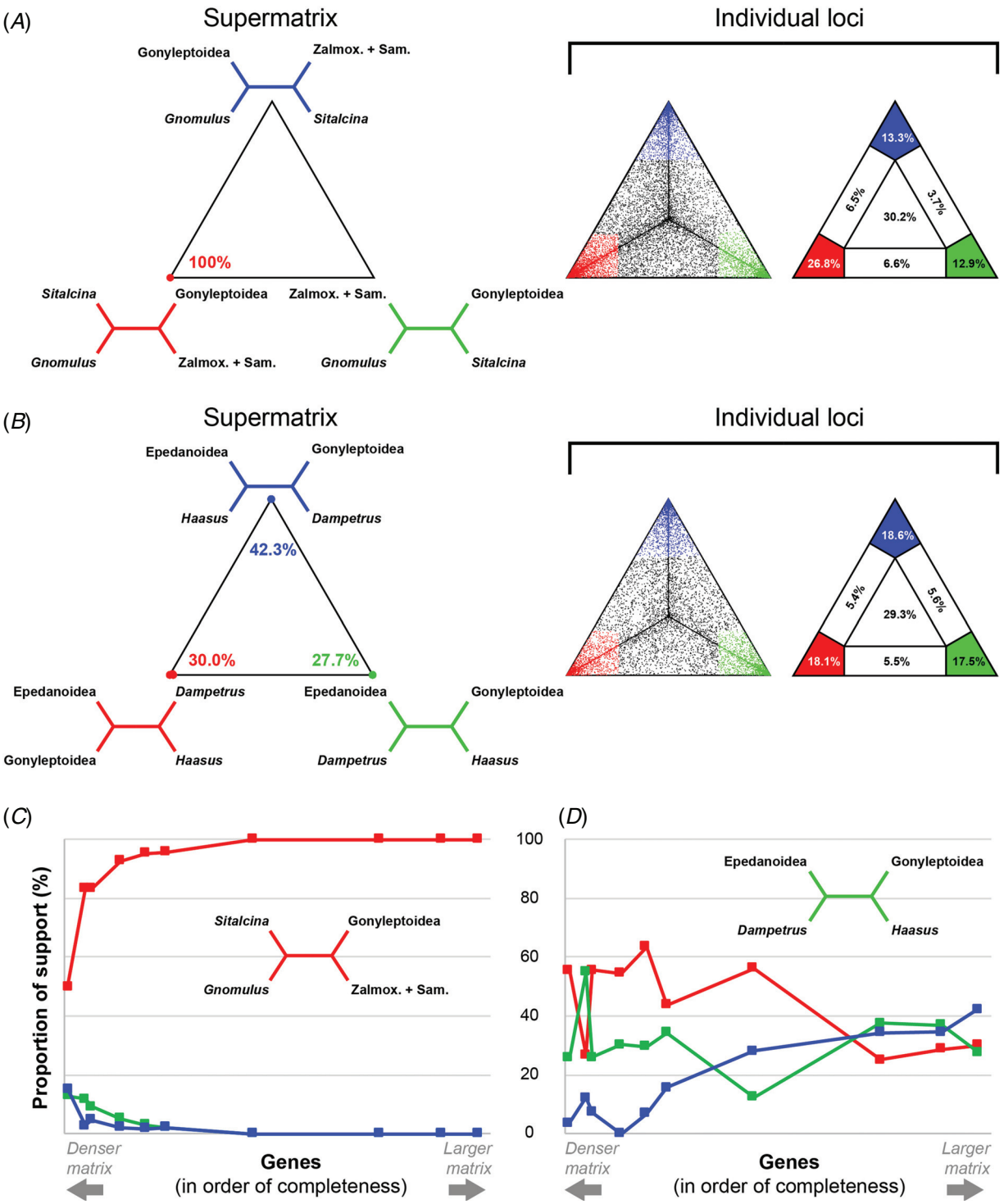

Fig. 9. Visualisation of conflicts in the phylogenetic signal by using four-cluster likelihood mapping. Three alternative statements are provided for each of two nodes, pertaining to (*A*) the non-controversial quartet *Sitalcina–Gnomulus*–Gonyleptoidea–Zalmoxoidea/Samooidea, and (*B*) the conflicting quartet *Haasus–Dampetrus*–Epedanoidea–Gonyleptoidea. (*A*) Distribution of resolved quartets recovered by 1550-locus supermatrix for the first node (left). Distribution of resolved quartets recovered by individual loci within the 1550-locus dataset for the first node (right). (*B*) Corresponding analyses as in *A*, for the second node. (*C*) Distribution of resolved quartets clearly supporting each topology, as a function of increasing matrix size (in a decreasing order of taxon occupancy), for the first node. (*D*) Corresponding analysis as in *C*, for the second node.

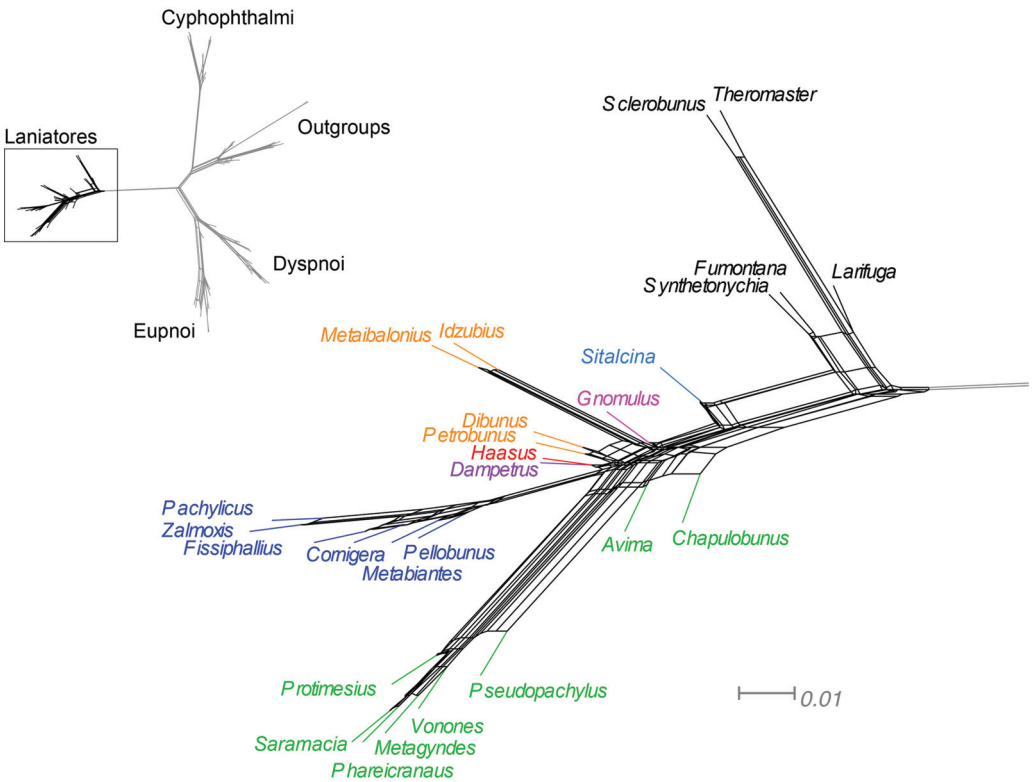

Fig. 10. Supernetwork representation of quartets derived from individual maximum-likelihood (ML) gene trees for the 1550-locus dataset. Phylogenetic conflict is represented by reticulations. Edge lengths correspond to quartet frequencies.

which is externally similar to *P. sauteri* in lacking a sexually dimorphic male trochanter IV. As with *Haasus*, the phylogenetic placement of *P. sauteri* in our study alters a long-held biogeographic scenario centred around the interpretation of a putative Holarctic distribution, suggesting instead a pattern of *in situ* diversification in eastern Asia and the Sunda Shelf. We transfer *Proscotolemon* to Petrobunidae (*new familial assignment*).

The characterisation of Phalangodidae as Laurasian has, therefore, become progressively untenable. As presently defined, the distribution of Phalangodidae may reflect a Pangean fauna that has lost much of its distribution in South America. This interpretation is consistent with the previously estimated Late Triassic age of the split between *Remyus* and the Holarctic genera *Bishopella* and *Scotolemon* (Sharma and Giribet 2011; this study, Fig. 8).

The anatomy of a conflict

Laniatores is atypical among the suborders of Opiliones in that its phylogenetic backbone bears five short internodes that diverge in a quick succession at the base of Grassatores. Such divergences have proven challenging even for genome-scale datasets and often incur topologies that are highly sensitive to matrix composition and variation of analytical parameters, in tandem with high (or maximal) nodal-support values for mutually exclusive hypotheses (Sharma *et al*. 2014; Kocot *et al*. 2016; Feuda *et al*. 2017; Laumer *et al*. 2018; Pease *et al*. 2018). For this reason, the characterisation of harvestman phylogeny as 'robust' and 'stable' by Fernández *et al*. (2017) is better suited to subordinal relationships and most relationships within Phalangida. Yet, a cursory glance at the sensitivity analysis from that work (fig. S1 of Fernández *et al*. 2017) shows several nodes that are unstable across analyses; within Laniatores, these consist of the placement of Assamiidae, the monophyly and internal relationships of Epedanoidea, and the root of Gonyleptoidea. Ironically, the placement and resolution of Sironidae (the Cyphophthalmi family upheld as the epitome of a Laurasian harvestman group) was also similarly unstable across analyses in Fernández *et al*. (2017). Notably, neither Pyramidopidae nor Tithaeidae (an epedanoid family of uncertain phylogenetic affinity; Sharma and Giribet 2011; Sharma *et al*. 2017) were sampled in that analysis.

On discovering that *Haasus* was a pyramidopid, we re-examined the phylogenomics of Laniatores to assess its placement, with the expectation that adding a pyramidopid to this analysis should improve the stability of basal Laniatores relationships. Intriguingly, the addition of a single family-level terminal with high data availability to a reasonably stable phylogenetic dataset destabilised the basal (i.e. superfamilial) topology of Grassatores, with concatenation approaches using the largest and sparsest supermatrices supporting the clade Pyramidopidae + Gonyleptoidea with maximal nodal support (Fig. 8*A*, *B*), and datasets of intermediate density recovering the traditional Assamioidea (Pyramidopidae + Assamiidae), with high nodal support. By contrast, gene-tree reconciliation

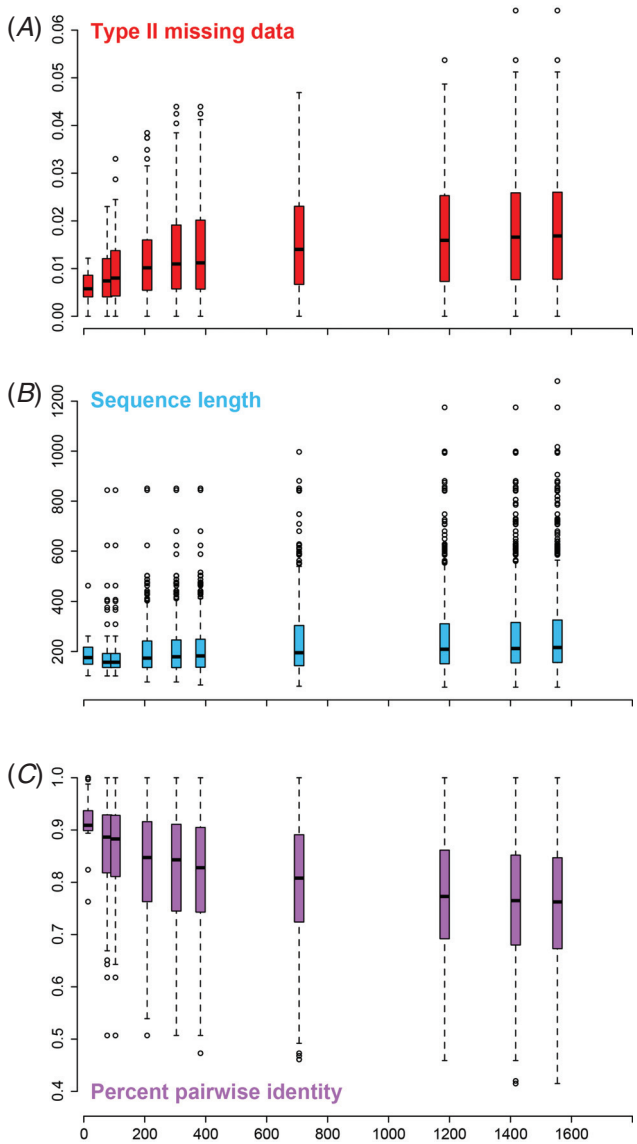

Fig. 11. Boxplots of (*A*) Type II missing data, (*B*) locus length, and (*C*) percentage pairwise identity for loci within each of 10 matrices, assembled using decreasing thresholds for taxon occupancy. The densest matrix contains significantly shorter, more conserved loci than do matrices with ≥304 genes (Whitney–Mann test; $P < 0.005$).

approaches using ASTRAL-II never recovered the former topology, or did so with <50% nodal support. This present work, thus, constitutes an interesting case study, wherein increasing taxonomic sampling counterintuitively worsens phylogenetic uncertainty. This phenomenon stands in stark contrast to other nodes in the Opiliones Tree of Life, which are, indeed, robustly resolved and accrue support monotonically on sequential addition of genes, even if those additional partitions are comparatively sparse, which is the pattern expected for nodes that are phylogenetically accurate.

Supermatrices can be assembled according to different criteria (e.g. taxon occupancy, rate of evolution, compositional heterogeneity), with compositional heterogeneity and missing data, in particular, drawing attention in recent analyses of short, deep internodes (Hosner *et al*. 2016; Feuda *et al*. 2017; Laumer *et al*. 2018; Parks *et al*. 2018). In the present case, compositional heterogeneity tends not to affect lineages as derived as the Laniatores; although this source of bias was explored using BaCoCa v. 1.1 (Kück and Struck 2014), none of the partitions or taxa was found to be aberrant, which is consistent with the investigations of Fernández *et al*. (2017) (not shown, data available on request).

We, therefore, turned our attention to missing data in the form of entire loci absent in a partition (Type I missing data *sensu* Hosner *et al*. 2016), which is widespread in transcriptomic datasets. On ordering all loci in the dataset for completeness (from most complete to least complete), we assessed whether the ensuing supermatrices had comparable sequence lengths, rates of evolution (measured using percentage pairwise identity; Sharma *et al*. 2014), and Type II missing data (i.e. sequences of partial length; Hosner *et al*. 2016). The last of these has been shown to engender incongruence between concatenation and gene-tree reconciliation approaches (Hosner *et al*. 2016). Notably, in their study, Hosner *et al*. (2016) encountered a simpler variant of the problem posed herein, with nodes being monotonically supported by the addition of sparser datasets (exemplified by the node in Fig. 9*C*); Hosner *et al*. (2016) were principally concerned with the discrepancy between concatenation methods and species trees for short internodes.

However, we found that truncated sequences were not a significant contributor to bias in our analysis (*contra* analyses of UCE datasets; Hosner *et al*. 2016); the average proportion of missing data (gaps) across all loci in the present study was 0.0176 ($\sigma = 0.012$), with a maximum value of 0.0641. The prevalence of Type II missing data was correlated with taxon occupancy, with sparser matrices also bearing more incomplete sequences (Fig. 11*A*); however, because all datasets had been masked to omit ambiguously aligned regions, no locus had more than 6.5% Type II missing data.

Of greater concern is the discovery that the most complete matrices tended to consist of significantly shorter loci than did matrices with ≥304 genes (Whitney–Mann test; $P < 0.005$; Fig. 11*B*). A separate troubling trend observed herein was that the most complete partitions also exhibited a higher percentage pairwise identity, bordering on completely uninformative partitions (Fig. 11*C*; Matrix 9 in Fig. 8). A trade-off, therefore, exists in this phylotranscriptomic dataset between (1) creating a denser matrix of short, less informative loci, and (2) incorporating sparser datasets with more informative sites.

The anatomy of instability

Phylogenetic instability in this region of Laniatores phylogeny could stem from two causes, namely, uninformative partitions or a conflict between partitions (Nieselt-Struwe and Haeseler von 2001; Pease *et al*. 2018). Four-cluster likelihood analyses of seven supermatrices varying by taxon-occupancy threshold showed that the instability of pyramidopid placement is clearly attributable to conflicting tree topologies (Fig. 9*A*, *B*). Most of the individual partitions proved uninformative for the node in question; however, this is typical for empirical

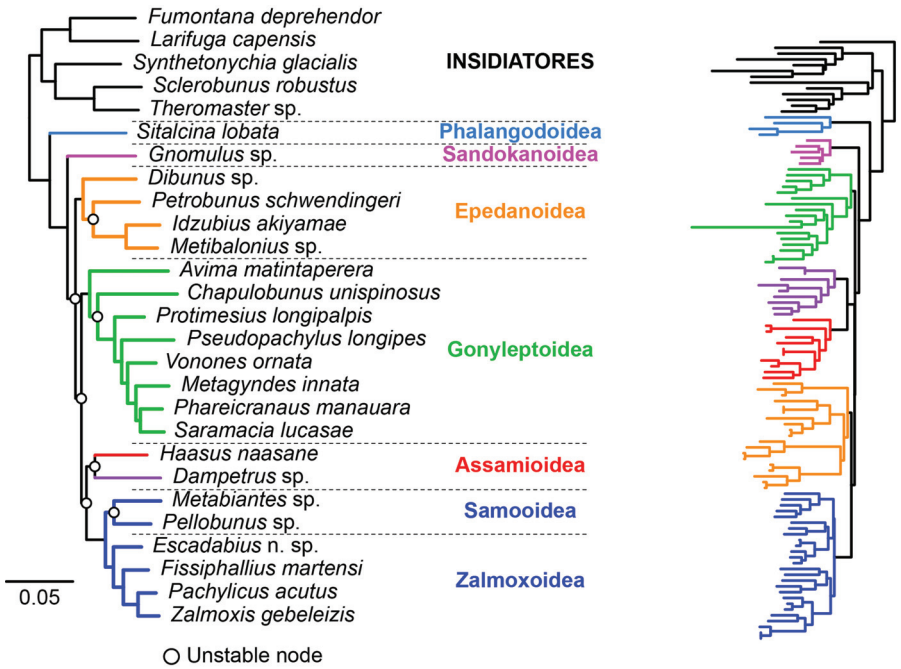

Fig. 12. Preferred topology of Laniatores higher-level relationships on the basis of a maximum likelihood-analysis of the 210-locus dataset. This matrix is selected for its balance of taxon occupancy and matrix size. White circles indicate unstable nodes that require further investigation. Right, maximum-likelihood tree topology from Fig. 6, showing congruence in superfamilial composition, but not superfamilial relationships.

phylogenies. Nevertheless, we note here that two of the partitions employed by Fernández *et al*. (2017), orthogroups 3965 and 51 085, comprised only invariable sites, with the latter of these appearing in all our matrices; although they were retained here for comparability of analysis of this dataset, such partitions do not contribute anything to phylogenetic analyses. In the specific case of partition-free analyses such as the ones employed by (Fernández *et al*. 2017), such as PhyML–PCMA, invariable partitions can additionally skew the estimation of model parameters.

Regardless, the startling outcome for the placement of Pyramidopidae is that none of the alternative topologies was significantly favoured by individual partitions, and one partition that was never obtained by concatenation methods was the best supported by the largest supermatrix (Matrix 3; Fig. 9*B*). Significant likelihood values for two competing hypotheses (corresponding to Assamioidea (= Pyramidopidae + Assamiidae) and the clade Pyramidopidae + Gonyleptoidea) were obtained in the denser matrices (Fig. 9*D*), with abrogation of likelihood differentials for any hypothesis on addition of sparser partitions (Fig. 9*D*). These patterns starkly contrast their counterparts for a stable and robustly supported node (Fig. 9*C*). Notably, these two nodes are comparable in phylogenetic depth, taxonomic sampling and data availability, with the highest taxon occupancy occurring in the terminals *Sitalcina lobata* (1449/1550 loci) and *Haasus naasane* sp. nov. (1540/1550 loci), and a single representative for each of two branches in both nodes (Phalangodidae and Sandokanidae, Fig. 9*A*; Assamiidae and Pyramidopidae, Fig. 9*B*).

Comparable dynamics have been observed for a short internode within the superfamily Ischyropsalidoidea (Richart *et al*. 2016). In that study, ML analyses of randomly concatenated supermatrices (Narechania *et al*. 2012; phylogenomic subsampling, *sensu* Edwards 2016) recovered support for one of two competing hypotheses after datasets exceeded 400 loci in size. However, nodal support inferred under two gene-tree reconciliation methods for the same datasets suggested persistent conflict, with values of support never exceeding 80% for even the largest matrices. The conclusion that Richart *et al*. (2016) drew from these patterns was that the concatenation approach was more robust than were multispecies coalescent approaches in that concatenated matrices show a hidden signal across distant partitions. This work was, subsequently, critiqued by Edwards (2016) on the grounds that variation of support values within random subsamples was not taken into account. On re-analysis of the nodal-support trajectories produced by Richart *et al*. (2016), Edwards (2016) also observed that the supermatrix approach, contrary to its characterisation by Richart *et al*. (2016), was more prone to overestimating support for topologies than were gene-tree reconciliation approaches, with the key difference that Edwards (2016) adopted a higher threshold to consider a node supported. Even though the interrogative approaches employed by Richart *et al*. (2016) and the present study are comparable, we drew opposite conclusions; to us, maximal nodal-support values obtained in supermatrix approaches cannot be taken as synonymous with phylogenetic resolution, topological accuracy, or efficiency of the supermatrix approach

in revealing the hidden signal. As shown in the present study, the maximal nodal support obtained for the relationship Pyramidopidae + Gonyleptoidea reflects only the amplification of noise across a large, patchy dataset.

In other parts of the Laniatores tree, nodal instability was attributable to clade-specific patterns of missing data. Uncertainty as to the identity of the sister group of the remaining Gonyleptoidea (either Agoristenidae (*Avima mantintaperera* (Pinto-da-Rocha, 1996)) or Stygnopsidae (*Chapulobunus unispinosus* Goodnight & Goodnight, 1946), or a clade of the two) is at least partially attributable to poor representation of these terminals in the matrix (Fig. 8). The same may be true of the internal relationships of Epedanoidea, given the poor representation of both podoctid species (*Metibalonius* sp. and *Idzubius akiyamae* Hirst, 1911).

The phylogenetic position of Pyramidopidae is, thus, demonstrably prone to instability and sensitivity to analytical framework implemented, despite interrogation with 1550 gene partitions, 401 342 aligned sites of peptide sequence data, and high representation in all matrices analysed.

Conclusions

The trade-off between dataset size and density is a problematic phenomenon for phylogenomic analyses. In the present case, either extreme is demonstrably undesirable. The densest matrix (>90% taxon occupancy) proved to be incapable of resolving relationships that even a Sanger dataset could recover (e.g. monophyly of superfamilies), owing to lack of informative loci in the most complete partitions (sensitivity plots in Fig. 8). At the other extreme, the largest matrix of all 1550 loci recovered maximal nodal support (Fig. 8) for a node plagued by systemic inter-partition conflict (Fig. 9*B*, *D*). The results presented herein are mystifying because there is no clear consensus on how such topological conflict should be adjudicated (Salichos and Rokas 2013; Sharma *et al*. 2014; Kocot *et al*. 2016; Shen *et al*. 2017), much less where the trade-off between the phylogenomic supermatrix size and density is optimised when Type I missing data are present (Wiens and Tiu 2012; Roure *et al*. 2013). As a compromise, we selected as our preferred topology the 210-locus dataset (19.9% missing data; Fig. 12). This topology is congruent with the more richly sampled 10-locus Sanger legacy dataset with respect to the monophyly of Assamioidea and the composition of other superfamilies, but differs markedly with respect to relationships among the non-sandokanid tropical Grassatores. We, additionally, have highlighted various nodes in the Laniatores tree of life that remain insufficiently stable to merit the epithets ‘resolved’ or ‘stable’ (*contra* Fernández *et al*. 2017; Fig. 12).

Phylotranscriptomic efforts to resolve the basal relationships of Laniatores should emphasise the following four strategies: (1) increasing taxonomic sampling to match or surpass that of legacy datasets; (2) utilising a topology aware-orthology search strategy that demonstrably outperforms OMA (the software used by Fernández *et al*. (2017) to erect this dataset; Altenhoff and Dessimoz 2009; Altenhoff *et al*. 2013) with respect to number of orthologs identified, such as the phylogenetically informed alternative UPhO (Ballesteros and Hormiga 2016); (3) incorporating dissection of inter-partition conflict when topological instability is evident; and (4) establishing *a priori* bright-line criteria for the designation of a given node as ‘resolved’.

Conflicts of interests

The authors declare no conflicts of interest.

Declaration of funding

This study was supported by the Israel Taxonomy Initiative (ITI) visiting scientist grant to PPS, and ITI and HUJ fellowships to SA. Fieldwork in Israel was supported by a National Geographic Society Expeditions Council grant NGS-271R-18 to JAB and PPS.

Acknowledgements

We thank the Israel National Parks Authority for issuing collection permits (2017/41718) to EGR and the Israel Cave Research Center (ICRC), and especially Amos Frumkin, for assistance in the field and valuable discussions. Assaf Uzan and Akiva Toper facilitated photography of type specimens. Scanning electron microscopy was performed at the Newcomb Imaging Center, Department of Botany, University of Wisconsin-Madison. Sequencing was performed at the Biotechnology Center at the University of Wisconsin-Madison and supported by National Science Foundation grant IOS-1552610. Comments from the Editor and one anonymous reviewer improved an earlier draft of the manuscript.

References

Aberer, A. J., Kobert, K., and Stamatakis, A. (2014). ExaBayes: massively parallel Bayesian tree inference for the whole-genome era. *Molecular Biology and Evolution* **31**, 2553–2556. doi:10.1093/molbev/msu236

Altenhoff, A. M., and Dessimoz, C. (2009). Phylogenetic and functional assessment of orthologs inference projects and methods. *PLoS Computational Biology* **5**, e1000262. doi:10.1371/journal.pcbi.1000262

Altenhoff, A. M., Gil, M., Gonnet, G. H., and Dessimoz, C. (2013). Inferring hierarchical orthologous groups from orthologous gene pairs. *PLoS One* **8**, e53786. doi:10.1371/journal.pone.0053786

Avni, Y., Filin S., and Zilberman E. (2012). The evolution of Nahal Ze’elim fan and recommendations for the emplacement of new infrastructures in the fan area [in Hebrew], Geological Survery of Israel Report GSI/3/2012, 52 p.

Ballesteros, J. A., and Hormiga, G. (2016). A new orthology assessment method for phylogenomic data: unrooted phylogenetic orthology. *Molecular Biology and Evolution* **33**, 2117–2134. doi:10.1093/molbev/msw069

Boyer, S. L., Clouse, R. M., Benavides, L. R., Sharma, P., Schwendinger, P. J., Karunarathna, I., and Giribet, G. (2007). Biogeography of the world: a case study from cyphophthalmid Opiliones, a globally distributed group of arachnids. *Journal of Biogeography* **34**, 2070–2085. doi:10.1111/j.1365-2699.2007.01755.x

Castresana, J. (2000). Selection of conserved blocks from multiple alignments for their use in phylogenetic analysis. *Molecular Biology and Evolution* **17**, 540–552. doi:10.1093/oxfordjournals.molbev.a026334

Cruz-López, J. A., Proud, D. N., and Pérez-González, A. (2016). When troglomorphism dupes taxonomists: morphology and molecules reveal the first pyramidopid harvestman (Arachnida, Opiliones, Pyramidopidae) from the New World. *Zoological Journal of the Linnean Society* **177**, 602–620. doi:10.1111/zoj.12382

Dequeiroz, A., and Gatesy, J. (2007). The supermatrix approach to systematics. *Trends in Ecology & Evolution* **22**, 34–41. doi:10.1016/j.tree.2006.10.002

Drummond, A. J., and Rambaut, A. (2007). BEAST: Bayesian evolutionary analysis by sampling trees. *BMC Evolutionary Biology* **7**, 214–218. doi:10.1186/1471-2148-7-214

Drummond, A. J., Ho, S. Y. W., Phillips, M. J., and Rambaut, A. (2006). Relaxed phylogenetics and dating with confidence. *PLoS Biology* **4**, e88. doi:10.1371/journal.pbio.0040088

Dunlop, J. A., Anderson, L. I., Kerp, H., and Hass, H. (2003*a*). Preserved organs of Devonian harvestmen. *Nature* **425**, 916. doi:10.1038/425916a

Dunlop, J., Anderson, L., Kerp, H., and Hass, H. (2003*b*). A harvestman (Arachnida: Opiliones) from the Early Devonian Rhynie cherts, Aberdeenshire, Scotland. *Transactions of the Royal Society of Edinburgh. Earth Sciences* **94**, 341–354. doi:10.1017/S0263593300000730

Edgar, R. C. (2004). MUSCLE: multiple sequence alignment with high accuracy and high throughput. *Nucleic Acids Research* **32**, 1792–1797. doi:10.1093/nar/gkh340

Edwards, S. V. (2016). Phylogenomic subsampling: a brief review. *Zoologica Scripta* **45**, 63–74. doi:10.1111/zsc.12210

Fernández, R., Sharma, P. P., Tourinho, A. L., and Giribet, G. (2017). The Opiliones tree of life: shedding light on harvestmen relationships through transcriptomics. *Proceedings of the Royal Society B: Biological Sciences* **284**, 20162340. doi:10.1098/rspb.2016.2340

Feuda, R., Dohrmann, M., Pett, W., Philippe, H., Rota-Stabelli, O., Lartillot, N., Worheide, G., and Pisani, D. (2017). Improved modeling of compositional heterogeneity supports sponges as sister to all other animals. *Current Biology* **27**, 3864–3870.e4. doi:10.1016/j.cub.2017.11.008

Frumkin, A., Langford, B., and Porat, R. (2017). The Judean Desert: the major hypogene cave region of the southern Levant. In 'Hypogene Karst Regions and Caves of the World'. (Eds A. Klimchouk, A. N. Palmer, J. De Waele, A. S. Auler, and P. Audra.) pp. 463–477. (Springer: Cham, Switzerland.)

Frumkin, A., Aharon, S., Davidovich, U., Langford, B., Negev, Y., Ullman, M., Vaks, A., Ya'aran, S., and Zissu, B. (2018). Old and recent processes in a warm and humid desert hypogene cave: 'A'rak Na'asane, Israel. *International Journal of Speleology* **47**, 307–321. doi:10.5038/1827-806X.47.3.2178

Garwood, R. J., Dunlop, J. A., Giribet, G., and Sutton, M. D. (2011). Anatomically modern carboniferous harvestmen demonstrate early cladogenesis and stasis in Opiliones. *Nature Communications* **2**, 444. doi:10.1038/ncomms1458

Garwood, R. J., Sharma, P. P., Dunlop, J. A., and Giribet, G. (2014). A Paleozoic stem group to mite harvestmen revealed through integration of phylogenetics and development. *Current Biology* **24**, 1017–1023. doi:10.1016/j.cub.2014.03.039

Gatesy, J., and Springer, M. S. (2014). Phylogenetic analysis at deep timescales: unreliable gene trees, bypassed hidden support, and the coalescence/concatalescence conundrum. *Molecular Phylogenetics and Evolution* **80**, 231–266. doi:10.1016/j.ympev.2014.08.013

Giribet, G., and Boyer, S. (2002). A cladistic analysis of the cyphophthalmid genera (Opiliones, Cyphophthalmi). *The Journal of Arachnology* **30**, 110–128. doi:10.1636/0161-8202(2002)030[0110:ACAOTC]2.0.CO;2

Giribet, G., and Kury, A. B. (2007). Phylogeny and biogeography. In 'Harvestmen: the biology of Opiliones'. (Eds R. Pinto-da-Rocha, G. Machado, and G. Giribet.) pp. 62–87. (Harvard University Press: Cambridge, MA, USA.)

Giribet, G., Rambla, M., Carranza, S., Baguñà, J., Riutort, M., and Ribera, C. (1999). Phylogeny of the arachnid order Opiliones (Arthropoda) inferred from a combined approach of complete 18S and partial 28S ribosomal DNA sequences and morphology. *Molecular Phylogenetics and Evolution* **11**, 296–307. doi:10.1006/mpev.1998.0583

Giribet, G., Edgecombe, G. D., Wheeler, W. C., and Babbitt, C. (2002). Phylogeny and systematic position of Opiliones: a combined analysis of chelicerate relationships using morphological and molecular data. *Cladistics* **18**, 5–70. doi:10.1006/clad.2001.0185

Giribet, G., Vogt, L., González, A. P., Sharma, P., and Kury, A. B. (2010). A multilocus approach to harvestman (Arachnida: Opiliones) phylogeny with emphasis on biogeography and the systematics of Laniatores. *Cladistics* **26**, 408–437. doi:10.1111/j.1096-0031.2009.00296.x

Giribet, G., Sharma, P. P., Benavides, L. R., Boyer, S. L., Clouse, R. M., de Bivort, B. L., Dimitrov, D., Kawauchi, G. Y., Murienne, J., and Schwendinger, P. J. (2012). Evolutionary and biogeographical history of an ancient and global group of arachnids (Arachnida: Opiliones: Cyphophthalmi) with a new taxonomic arrangement. *Biological Journal of the Linnean Society. Linnean Society of London* **105**, 92–130. doi:10.1111/j.1095-8312.2011.01774.x

Gouy, M., Guindon, S., and Gascuel, O. (2010). SeaView Version 4: a multiplatform graphical user interface for sequence alignment and phylogenetic tree building. *Molecular Biology and Evolution* **27**, 221–224. doi:10.1093/molbev/msp259

Grabherr, M. G., Haas, B. J., Yassour, M., Levin, J. Z., Thompson, D. A., Amit, I., Adiconis, X., Fan, L., Raychowdhury, R., Zeng, Q., Chen, Z., Mauceli, E., Hacohen, N., Gnirke, A., Rhind, N., Di Palma, F., Birren, B. W., Nusbaum, C., Lindblad-Toh, K., Friedman, N., and Regev, A. (2011). Full-length transcriptome assembly from RNA-Seq data without a reference genome. *Nature Biotechnology* **29**, 644–652. doi:10.1038/nbt.1883

Grünewald, S., Spillner, A., Bastkowski, S., Bogershausen, A., and Moulton, V. (2013). SuperQ: computing supernetworks from quartets. *IEEE/ACM Transactions on Computational Biology and Bioinformatics* **10**, 151–160. doi:10.1109/TCBB.2013.8

Hedin, M., and Thomas, S. M. (2010). Molecular systematics of eastern North American Phalangodidae (Arachnida: Opiliones: Laniatores), demonstrating convergent morphological evolution in caves. *Molecular Phylogenetics and Evolution* **54**, 107–121. doi:10.1016/j.ympev.2009.08.020

Hedin, M., Starrett, J., Akhter, S., Schönhofer, A. L., and Shultz, J. W. (2012). Phylogenomic resolution of Paleozoic divergences in harvestmen (Arachnida, Opiliones) via analysis of next-generation transcriptome data. *PLoS One* **7**, e42888. doi:10.1371/journal.pone.0042888

Hoang, D. T., Chernomor, O., von Haeseler, A., Minh, B. Q., and Vinh, L. S. (2018). UFBoot2: improving the ultrafast bootstrap approximation. *Molecular Biology and Evolution* **35**, 518–522. doi:10.1093/molbev/msx281

Hosner, P. A., Faircloth, B. C., Glenn, T. C., Braun, E. L., and Kimball, R. T. (2016). Avoiding missing data biases in phylogenomic inference: an empirical study in the landfowl (Aves: Galliformes). *Molecular Biology and Evolution* **33**, 1110–1125. doi:10.1093/molbev/msv347

Kalyaanamoorthy, S., Minh, B. Q., Wong, T. K. F., von Haeseler, A., and Jermiin, L. S. (2017). ModelFinder: fast model selection for accurate phylogenetic estimates. *Nature Methods* **14**, 587–589. doi:10.1038/nmeth.4285

Kocot, K. M., Struck, T. H., Merkel, J., Waits, D. S., Todt, C., Brannock, P. M., Weese, D. A., Cannon, J. T., Moroz, L. L., Lieb, B., and Halanych, K. M. (2016). Phylogenomics of Lophotrochozoa with consideration of systematic error. *Systematic Biology* **151**, syw079–syw27. doi:10.1093/sysbio/syw079

Kozlov, A. M., Aberer, A. J., and Stamatakis, A. (2015). ExaML version 3: a tool for phylogenomic analyses on supercomputers. *Bioinformatics* **31**, 2577–2579. doi:10.1093/bioinformatics/btv184

Kück, P., and Struck, T. H. (2014). BaCoCa: a heuristic software tool for the parallel assessment of sequence biases in hundreds of gene and taxon partitions. *Molecular Phylogenetics and Evolution* **70**, 94–98. doi:10.1016/j.ympev.2013.09.011

Laumer, C. E., Gruber-Vodicka, H., Hadfield, M. G., Pearse, V. B., Riesgo, A., Marioni, J. C., and Giribet, G. (2018). Support for a clade of Placozoa

and Cnidaria in genes with minimal compositional bias. *eLife* **7**, e36278. doi:10.7554/eLife.36278

Linkem, C. W., Minin, V. N., and Leaché, A. D. (2016). Detecting the anomaly zone in species trees and evidence for a misleading signal in higher-level skink phylogeny (Squamata: Scincidae). *Systematic Biology* **65**, 465–477. doi:10.1093/sysbio/syw001

Minh, B. Q., Nguyen, M. A. T., and Haeseler Von, A. (2013). Ultrafast approximation for phylogenetic bootstrap. *Molecular Biology and Evolution* **30**, 1188–1195. doi:10.1093/molbev/mst024

Mirarab, S., and Warnow, T. (2015). ASTRAL-II: coalescent-based species tree estimation with many hundreds of taxa and thousands of genes. *Bioinformatics* **31**, i44–i52. doi:10.1093/bioinformatics/btv234

Mor, D. (1993). A time-table for the Levant volcanic province, according to K-Ar dating in the Golan heights, Israel. *Journal of African Earth Sciences* **16**, 223–234. doi:10.1016/0899-5362(93)90044-Q

Murphree, C. S. (1988). Morphology of the dorsal integument of 10 opilionid species (Arachnida, Opiliones). *The Journal of Arachnology* **16**, 237–252.

Narechania, A., Baker, R. H., Sit, R., Kolokotronis, S.-O., DeSalle, R., and Planet, P. J. (2012). Random addition concatenation analysis: a novel approach to the exploration of phylogenomic signal reveals strong agreement between core and shell genomic partitions in the cyanobacteria. *Genome Biology and Evolution* **4**, 30–43. doi:10.1093/gbe/evr121

Nguyen, L.-T., Schmidt, H. A., Haeseler von, A., and Minh, B. Q. (2015). IQ-TREE: a fast and effective stochastic algorithm for estimating maximum-likelihood phylogenies. *Molecular Biology and Evolution* **32**, 268–274. doi:10.1093/molbev/msu300

Nieselt-Struwe, K., and Haeseler Von, A. (2001). Quartet-mapping, a generalization of the likelihood-mapping procedure. *Molecular Biology and Evolution* **18**, 1204–1219. doi:10.1093/oxfordjournals.molbev.a003907

Oberski, J. T., Sharma, P. P., Jay, K. R., Coblens, M. J., Lemon, K. A., Johnson, J. E., and Boyer, S. L. (2018). A dated molecular phylogeny of mite harvestmen (Arachnida: Opiliones: Cyphophthalmi) elucidates ancient diversification dynamics in the Australian Wet Tropics. *Molecular Phylogenetics and Evolution* **127**, 813–822. doi:10.1016/j.ympev.2018.06.029

Parks, M. B., Wickett, N. J., and Alverson, A. J. (2018). Signal, uncertainty, and conflict in phylogenomic data for a diverse lineage of microbial eukaryotes (diatoms, Bacillariophyta). *Molecular Biology and Evolution* **35**, 80–93. doi:10.1093/molbev/msx268

Pease, J. B., Brown, J. W., Walker, J. F., Hinchliff, C. E., and Smith, S. A. (2018). Quartet sampling distinguishes lack of support from conflicting support in the green plant tree of life. *American Journal of Botany* **105**, 385–403. doi:10.1002/ajb2.1016

Rambaut, A., and Drummond, A. J. (2009). Tracer v. 1.7. Program and documentation. Available at http://tree.bio.ed.ac.uk/software/tracer/ [verified 10 July 2018].

Richart, C. H., Hayashi, C. Y., and Hedin, M. (2016). Phylogenomic analyses resolve an ancient trichotomy at the base of Ischyropsalidoidea (Arachnida, Opiliones) despite high levels of gene tree conflict and unequal minority resolution frequencies. *Molecular Phylogenetics and Evolution* **95**, 171–182. doi:10.1016/j.ympev.2015.11.010

Roewer, C. F. (1949). Uber Phalangodiden I. *Senckenbergiana* **30**, 11–61.

Rokas, A. (2005). More genes or more taxa? The relative contribution of gene number and taxon number to phylogenetic accuracy. *Molecular Biology and Evolution* **22**, 1337–1344. doi:10.1093/molbev/msi121

Ronquist, F., Teslenko, M., Van Der Mark, P., Ayres, D. L., Darling, A., Höhna, S., Larget, B., Liu, L., Suchard, M. A., and Huelsenbeck, J. P. (2012). MrBayes 3.2: efficient Bayesian phylogenetic inference and model choice across a large model space. *Systematic Biology* **61**, 539–542. doi:10.1093/sysbio/sys029

Roure, B., Baurain, D., and Philippe, H. (2013). Impact of missing data on phylogenies inferred from empirical phylogenomic data sets. *Molecular Biology and Evolution* **30**, 197–214. doi:10.1093/molbev/mss208

Salichos, L., and Rokas, A. (2013). Inferring ancient divergences requires genes with strong phylogenetic signals. *Nature* **497**, 327–331. doi:10.1038/nature12130

Schmidt, S. M., Buenavente, P. A. C., Blatchley, D. D., Diesmos, A. C., Diesmos, M. L., General, D. E. M., Mohagan, A. B., Mohagan, D. J., Clouse, R. M., and Sharma, P. P. (2019). A new species of Tithaeidae (Arachnida: Opiliones: Laniatores) from Mindanao reveals contemporaneous colonization of the Philippines by Sunda Shelf opiliofauna. *Invertebrate Systematics* **33**, 237–251. doi:10.1071/IS18057

Schwentner, M., Combosch, D. J., Nelson, J. P., and Giribet, G. (2017). A phylogenomic solution to the origin of insects by resolving Crustacean–Hexapod relationships. *Current Biology* **27**, 1818–1824. e5. doi:10.1016/j.cub.2017.05.040

Segev, A., Schattner, U., and Lyakhovsky, V. (2011). Middle-Late Eocene structure of the southern Levant continental margin—Tectonic motion versus global sea-level change. *Tectonophysics* **499**, 165–177.

Sharma, P., and Giribet, G. (2009). Sandokanid phylogeny based on eight molecular markers: the evolution of a southeast Asian endemic family of Laniatores (Arachnida, Opiliones). *Molecular Phylogenetics and Evolution* **52**, 432–447. doi:10.1016/j.ympev.2009.03.013

Sharma, P. P., and Giribet, G. (2011). The evolutionary and biogeographic history of the armoured harvestmen–Laniatores phylogeny based on ten molecular markers, with the description of two new families of Opiliones (Arachnida). *Invertebrate Systematics* **25**, 106–142. doi:10.1071/IS11002

Sharma, P. P., and Giribet, G. (2014). A revised dated phylogeny of the arachnid order Opiliones. *Frontiers in Genetics* **5**, 255. doi:10.3389/fgene.2014.00255

Sharma, P. P., Prieto, C., and Giribet, G. (2011). A new family of Laniatores (Arachnida: Opiliones) from the Afrotropics. *Invertebrate Systematics* **25**, 143–154. doi:10.1071/IS11003

Sharma, P. P., Kaluziak, S. T., Perez-Porro, A. R., Gonzalez, V. L., Hormiga, G., Wheeler, W. C., and Giribet, G. (2014). Phylogenomic interrogation of Arachnida reveals systemic conflicts in phylogenetic signal. *Molecular Biology and Evolution* **31**, 2963–2984. doi:10.1093/molbev/msu235

Sharma, P. P., Fernández, R., Esposito, L. A., Gonzalez-Santillan, E., and Monod, L. (2015). Phylogenomic resolution of scorpions reveals multilevel discordance with morphological phylogenetic signal. *Proceedings. Biological Sciences* **282**, 20142953. doi:10.1098/rspb.2014.2953

Sharma, P. P., Santiago, M. A., Kriebel, R., Lipps, S. M., Buenavente, P. A. C., Diesmos, A. C., Janda, M., Boyer, S. L., Clouse, R. M., and Wheeler, W. C. (2017). A multilocus phylogeny of Podoctidae (Arachnida, Opiliones, Laniatores) and parametric shape analysis reveal the disutility of subfamilial nomenclature in armored harvestman systematics. *Molecular Phylogenetics and Evolution* **106**, 164–173. doi:10.1016/j.ympev.2016.09.019

Shen, X.-X., Hittinger, C. T., and Rokas, A. (2017). Contentious relationships in phylogenomic studies can be driven by a handful of genes. *Nature Ecology & Evolution* **1**, 0126. doi:10.1038/s41559-017-0126

Shultz, J. W., and Regier, J. C. (2001). Phylogenetic analysis of Phalangida (Arachnida, Opiliones) using two nuclear protein-encoding genes supports monophyly of Palpatores. *The Journal of Arachnology* **29**, 189–200. doi:10.1636/0161-8202(2001)029[0189:PAOPAO]2.0.CO;2

Simmons, M. P., and Gatesy, J. (2015). Coalescence vs. concatenation: sophisticated analyses vs. first principles applied to rooting the angiosperms. *Molecular Phylogenetics and Evolution* **91**, 98–122. doi:10.1016/j.ympev.2015.05.011

Song, S., Liu, L., Edwards, S. V., and Wu, S. (2012). Resolving conflict in eutherian mammal phylogeny using phylogenomics and the multispecies coalescent model. *Proceedings of the National Academy of Sciences of the United States of America* **109**, 14942–14947. doi:10.1073/pnas.1211733109

Stamatakis, A. (2014). RAxML version 8: a tool for phylogenetic analysis and post-analysis of large phylogenies. *Bioinformatics* **30**, 1312–1313. doi:10.1093/bioinformatics/btu033

Stamatakis, A., Hoover, P., and Rougemont, J. (2008). A rapid bootstrap algorithm for the RAxML web servers. *Systematic Biology* **57**, 758–771. doi:10.1080/10635150802429642

Starega, W. (1973). Beitrag zur Kenntnis der Weberknechte (Opiliones) des Nahen Ostens. *Annales Zoologici* **30**, 129–153.

Steinitz, G., and Bartov, Y. (1992). The Miocene–Pleistocene history of the Dead Sea segment of the Rift in light of K-Ar ages of basalts. *Israel Journal of Earth Sciences* **38**, 199–208.

Tonini, J., Moore, A., Stern, D., Shcheglovitova, M., and Ortí, G. (2015). Concatenation and species tree methods exhibit statistically indistinguishable accuracy under a range of simulated conditions. *PLoS Currents* **1**, 1–16. doi:10.1371/currents.tol.34260cc27551a527b124ec5f6334b6be

Ubick, D. (2007). Phalangodidae Simon, 1879. In 'Harvestmen: the biology of Opiliones'. (Eds R. Pinto-da-Rocha, G. Machado, and G. Giribet.) pp. 217–221. (Harvard University Press: Cambridge, MA, USA.)

Wiens, J. J. (2006). Missing data and the design of phylogenetic analyses. *Journal of Biomedical Informatics* **39**, 34–42. doi:10.1016/j.jbi.2005.04.001

Wiens, J. J., and Tiu, J. (2012). Highly incomplete taxa can rescue phylogenetic analyses from the negative impacts of limited taxon sampling. *PLoS One* **7**, e42925. doi:10.1371/journal.pone.0042925

Zhang, C., Zhang, F., and Sharma, P. P. (2018). Two new species of *Petrobunus* from China (Opiliones: Laniatores: Petrobunidae). *Zootaxa* **4524**, 51–64. doi:10.11646/zootaxa.4524.1.3

Handling editor: Gonzalo Giribet